High Energy Electrode Materials for Lithium Sulfur Batteries

A thesis presented for the degree of Master of Science

By

Kefei Li

University of Technology, Sydney

Faculty of Science

March 2012

Certificate of Originality

I certify that the work in this thesis has not previously been submitted for a degree nor has it been submitted as part of requirements for a degree except as fully acknowledged within the text.

I also certify that the thesis has been written by me. Any help that I have received in my research work and the preparation of the thesis itself has been acknowledged. In addition, I certify that all information sources and literature used are indicated in the thesis.

Signature of Student

Production Note:
Signature removed prior to publication.

Kefei Li 05/03/2012

Acknowledgements

I would express my deep gratitude to my supervisor, Prof. Guoxiu Wang, for his consistent supervision and guidance throughout the whole period of my research work.

I also offer my regards to the staff members in School of Chemistry and Forensic Science, and Microstructural Analysis Unit who have provided essential assistance on the maintenance and operation of facilities. I am grateful to Dr. David Wexler who performed energy disperse spectroscopy elemental mapping on my behalf.

Special thanks to research students Bei Wang, Bing Sun, Dawei Su and Ying Wang in our group who have provided effective co-operation and generously shared their research experience with me.

Abstract

This thesis described the research work on high energy electrode materials for lithium sulfur batteries. The literature review of high energy electrode materials was presented, including the advantages and disadvantages of different anode and cathode materials and related synthesis techniques. The lithium-sulfur battery and sulfur cathode are the major focus due to their advantages in energy density, cost and environmental sustainability. Different sulfur cathodes based on amorphous carbon, graphene and mesoporous carbon were synthesized to study the correlation between morphology of carbonaceous material and the performance of the sulfur cathode. The as-prepared electrode materials have been characterized by X-ray diffraction, field emission scanning electron microscopy, backscattered imaging, energy disperse spectroscopy element mapping and thermogravimetric analysis. The synthesized sulfur composites are tested as cathode materials in subsequent electrochemical tests. The electrochemical tests performed on sulfur cathodes include cyclic voltammetry, galvanostatic charge-discharge cycle tests and electrochemical impedance measurements. The synthesized graphene-sulfur composite was tested as cathode material and achieved both high sulfur utilization rate with a high specific capacity of 1593 mAh /g and good rate capability at 1.0 C and 2.0 C discharge rates. Graphene within the sulfur composite greatly improved the electrochemical performance of Li-S battery. The effect of sulfur particle size and size distribution within the cathode to the performance of Li-S battery was

investigated through the synthesis of carbon-sulfur nanocomposite by an innovative solution-based synthesis technique. The modification of synthesis method has helped to reduce the particle size of sulfur to the level of about 200 nm. The as-prepared sulfur nanocomposite with a homogeneous dispersion of sulfur particles was applied as the cathode material in Li-S battery and exhibited a high reversible capacity of 1220 mAh/g and maintained favorable cycle stability.

Table of Content

List of Publications

Portions of the work presented in this thesis have been published, or have been submitted for publication. The following is a list of the citations for these publications:

Kefei Li, Bei Wang, Dawei Su, David Wexler, Hyojun Ahn, and Guoxiu Wang,

"Enhance electrochemical performance of lithium sulfur battery through a solution-based processing technique"

Journal of Power Sources, 2011, DOI information: 10.1016/j.jpowsour.2011.11.073

Bei Wang, **Kefei Li**, Dawei Su, David Wexler, Hyojun Ahn, and Guoxiu Wang,

"Superior electrochemical performance of sulfur/graphene nanocomposite material for high capacity lithium sulfur batteries"

Electrochimica Acta, 2011, submitted.

List of Abbreviations

LIB	Lithium-ion Battery
BEV	Battery-Electric Vehicle
ICEV	Internal-Combustion-Engine Vehicle
LOMO	Lowest Occupied Molecular Orbital
HOMO	Highest Occupied Molecular Orbital
Li-Air Battery	Lithium-Air Battery
Li-S Battery	Lithium-Sulfur Battery
XRD	X-ray diffraction
SEM	Scanning Electron Microscope
TGA	Thermogravimetric Analysis
CV	Cyclic Voltammetry
EIS	Electrochemical Impedance Spectroscopy
wt%	Weight Percent
MO	Metal Oxide
MS	Metal Sulfide
DMSO	Dimethyl Sulfoxide
DME	1,2-dimethoxyethane
DOX	1,3-dioxolane
TEGDME	Tetra(ethylene glycol)dimethyl ether
THF	Tetrahydrofuran
EMS	Ethyl methyl sulfone
DGDE	Diethylene glycol dimethyl ether
EC	Ethylene carbonate
DMC	Dimethyl carbonate
LiTFSI	$LiN(SO_2CF_3)_2$

List of Figures

1 Introduction

Lithium batteries were born from the tireless effort of many pioneers seeking light weight, compact electrical power sources in the last century. Military and space programs were in search for high performance battery systems that can work in a wide range of conditions. The fast advanced electronic technology results in the miniaturization of complex electronic devices which also requires battery systems with high energy density [1]. The demand of battery chemistry innovation constantly drives the development of battery systems. As a result, many primary lithium battery and secondary lithium battery systems have been successfully developed. Lithium is the lightest metal and possesses the lowest electronegativity of all metals. The high energy density and electronegativity of lithium metal makes it an ideal candidate as anode material for high energy battery system. However, the difficulty of developing rechargeable lithium battery system is mainly attributed to recharging lithium metal anode with suitable electrolytes and the formation of lithium dendrite at the electrode/electrolyte interface. Innovation of battery chemistry and electrode materials were conducted to overcome those difficulties. Investigations of ion conduction in solids revealed the possibility of creating a rechargeable battery system with lithium insertion compounds as the positive electrodes and energy can be stored and released in such electrodes through the lithium ion insertion/removal process. The similar lithium intercalation mechanisms

were also found on many kinds of carbonaceous materials including graphite. Hence the lithium metal anode can be replaced by graphite anode to avoid the problem of dendrite formation. The above discoveries eventually lead to the invention and development of lithium-ion batteries (LIBs) [2].

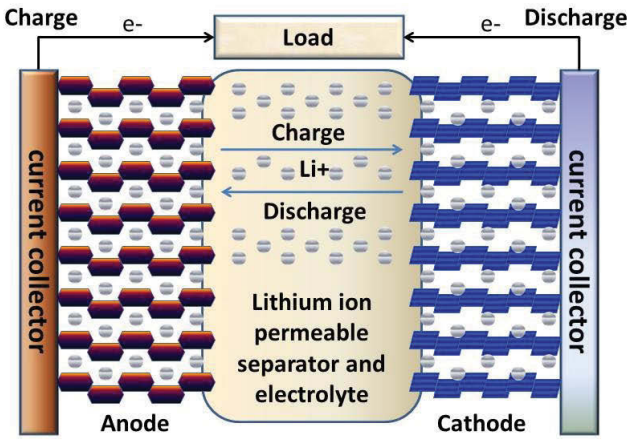

Figure 1.1 Schematic Configuration of Lithium-ion Battery

Figure 1.1 is a schematic illustration of lithium-ion battery (LIB). A typical LIB consists of graphite anode, lithium transition-metal oxide ($LiMO_2$) cathode and lithium ion conducting separator with non-aqueous electrolyte between two electrodes. The electrolyte is usually a solution of lithium salt in organic solvents. During the charge-discharge process, the lithium ions shuttle between positive and negative electrodes through electrolyte and separator. The intercalation process between graphite anode and lithium oxide cathode can be expressed in a simplified equation as follows:

$$6C + LiMO_2 \rightleftharpoons Li_xC_6 + Li_{(1-x)}MO_2 \quad (1.1)$$

The major improvement of LIB from preciously lithium batteries is the usage of lithium insertion materials as both positive and negative electrodes. The safety of LIB is enhanced because the lithium metal anode and related large scale dendrite formation no longer exists in this system. LIBs are the most successful commercialized secondary power sources among all kinds of lithium battery systems. LIBs are widely used in many fields including consumer electronics, medical, military and research applications due to its good capacity reversibility, relatively high energy and power densities.

As the development of battery system was proceeding, the troubled energy industry (carbon economy) was struggling with serious issues, including the growing energy demand, limited natural resources of fossil fuel, and the consequential environment pollution. Urge for economic growth will leads to rapid energy consumption increase worldwide in a foreseeable future. The fast climbing energy demands have caused many ecological concerns about the impact of carbon emission on global climate. Therefore, many efforts are devoted to the development of alternative clean energy sources and energy conversion and storage systems [3, 4]. Electrochemical systems including batteries and supercapacitors are essential intermittence of renewable energy resources because they are capable to restore

and deliver energy on demand. Compared with supercapacitors, lithium-ion batteries have higher energy densities and have attracted massive efforts on their research and development. The advancing technology of LIBs over the last two decades offered continuous improvement on energy density, power density and service lifetime. So far, the LIBs are the most promising electrochemical energy storage systems and the large scale applications of LIBs will play a key role in the evolution of energy industry.

However, the large scale application of LIBs, such as power sources for transportation vehicles and stationary energy storage, is currently impractical owing to the cost efficiency, safety, cycle life, energy and power density of LIBs [5]. Those attractive characteristics of LIB such as light weight, high energy densities compared with other electrochemical systems are much less significant in large scale applications. For instance, the major difference between the Battery-Electric Vehicle (BEV) and Internal-Combustion-Engine Vehicle (ICEV) is the power system. To replace the ICEVs with BEVs, the most important issue is that BEVs must have competitive market prices and reasonable operation per mileage. However, the high cost energy storage units in electrical powered vehicles definitely lead to increased manufacturing cost and operational cost. The limited cycle life of LIB requires regular replacement of battery units, which is another challenge for BEVs. The limited rate capability of LIBs and the consequential long charge time is another

negative factor on the performance of BEVs. Unlike the ICEVs which consume gasoline or diesel, the BEVs take hours to recharge before the power system can be functional again, this largely limits the range of applications of BEVs. Despite their inconvenience, the possible incidents of BEVs due to the safety hazards of LIB including risk of fire and explosion are even more serious.

The expanding markets of consumer electronics, BEVs drives the increasing demand of LIBs. However, the recycling technology of lithium from LIBs has yet to be established. The exhausting reserve of lithium worldwide would lead to the climbing market price of lithium batteries. Therefore, the energy density of LIBs must be increased in order to achieve the sustainable utilization of lithium reserves. In next chapter, I will present a literature review of research works on improvement of LIBs in terms of energy densities.

Chapter 2 is a literature review of research on materials and battery chemistry that have the potential to increase the energy density of rechargeable lithium battery to a higher level. Those materials include nanostructured carbonaceous anode materials, nanostructured metal oxide and metal sulfide anode materials. Lithium alloy anode materials are considered as electrode materials with high energy densities. A brief summary of advantages and disadvantages of the above materials are included. The innovative lithium-air battery and lithium-sulfur battery

configurations are described as modifications on battery chemistry, which are capable of utilizing the energy storage ability of lithium at a higher level in comparison with LIBs.

Chapter 3 covers the experiment procedures I used in this research project. The experiment techniques include material characterization and electrochemical tests. The materials were characterized by X-ray diffraction, scanning electron microscope, and thermogravimetric analysis. Electrochemical tests include cyclic voltammetry, impedance measurement and charge-discharge cycle tests. I presented two major approaches to synthesis sulfur composite materials: melt-diffusion (thermal) methods and solution-based methods. For solution-based synthesis method, I have utilized a new process optimized for dispersion of nanoscale sulfur particles in sulfur composite in order to improve the performance of lithium-sulfur batteries.

In Chapter 4, the thermal synthesis of sulfur composite with graphene nanosheets is described. The synthesized graphene-sulfur composite exhibits high sulfur utilization rate i.e. high specific capacity of sulfur and high rate capability as cathode material. X-ray diffraction was employed to investigate the phase transfer of sulfur during the synthesis process. Scanning electron microscope with energy dispersive spectroscopy elemental mapping revealed a relatively good sulfur distribution within the graphene-sulfur composite. The graphene-sulfur cathode materials

achieved a high initial specific discharge capacity of 1593 mAh/g[1] under 0.1C discharge rate, along with good sulfur utilization at 1.0 C and 2.0 C discharge rates.

Chapter 5 describes the works I have done on the synthesis of carbon-sulfur composite from a solution-based route and subsequent electrochemical test of as-prepared material as cathode. X-ray diffraction and scanning electron microscope were employed to examine the structural change of sulfur after the synthesis process. Backscattered image revealed a distribution of sulfur particles with varied sizes within the composite.

Chapter 6 describes the sonication synthesis of carbon-sulfur nanocomposite. The as-prepared sulfur nanocomposite also exhibits high sulfur utilization rate as cathode material. The modification of synthesis method with sonication and DMSO solvent has helped achieve the improvement in terms of cycle stability in comparison with previously synthesized sulfur composite described in Chapter 5. X-ray diffraction and scanning electron microscope were employed to examine the structural change of sulfur after the synthesis process. Backscattered image revealed the homogeneous distribution of sulfur within the composite. The as-prepared sulfur cathode materials achieved a high initial capacity of 1220 mAh/g under 0.1C discharge rate.

[1] The specific capacity of synthesized sulfur electrodes referred in this thesis are all calculated based on the weight of sulfur in the electrodes.

In Chapter 7, I presented the application of sonication-solution synthesis method on the combination of mesoporous carbon and sulfur. Due to the nature of mesoporous carbon, the sonication-solution route is ineffective in mesoporous carbon-sulfur composite synthesis. However, a mesoporous carbon-sulfur composite was successfully created through a thermal process and exhibit high coulombic efficiency.

At last, I concluded my research work in Chapter 8.

2 Literature Review

2.1 Components of Lithium-Ion Batteries

The performance of LIBs is affected by its three major components such as anode, electrolyte and cathode. Graphite is the common anode material used in LIBs due to its relatively high capacity retention rate. Although graphite is environmentally abundant and inexpensive resource, the process of graphite anode is complicated and costly. Graphite anode is the main factor that limits the energy density of LIBs and its low working potential also leads to safety hazards of LIBs. The energy capacity is determined by the saturation of lithium concentration in the electrode materials. The thermodynamic equilibrium of lithium ion saturation concentration in graphite is LiC_6 (See Eq. 1.1), which is equivalent to a theoretical capacity of 372 mAh/g. The topotactic intercalation mechanism of LIB limits the reversible capacity of any prospective LIB system with graphite anode to a maximum value at about 300 mAh/g.

Graphite is the choice of anode for LIB because its good cycle stability and low operating voltage. The operating voltage of graphite is close to that of Li^0/Li^+, which is good for extracting the energy storage ability of counter electrode. However, the low working voltage of graphite anode causes safety hazards in conjunction with the electrolytes currently used in LIBs. The electrochemical potential of graphite

exceeding the lowest unoccupied molecular orbital (LUMO) of the electrolyte leads to the reduction of the electrolyte and the formation of solid-electrolyte interfacial (SEI) layer [6], which result in the lithium plating on the surface of graphite, especially when the cell is under high charge-discharge rate. The lithium accumulation on the graphite surface increase the chance of lithium dendrite formation and penetration of cell separator, which result in the internal short circuit of battery and causes self-combustion and possible subsequent explosion of LIBs. Although the hazard level is low as ordinary LIBs are usually in small sizes, the magnification of this particular hazard will become fatal in large scale application of LIBs.

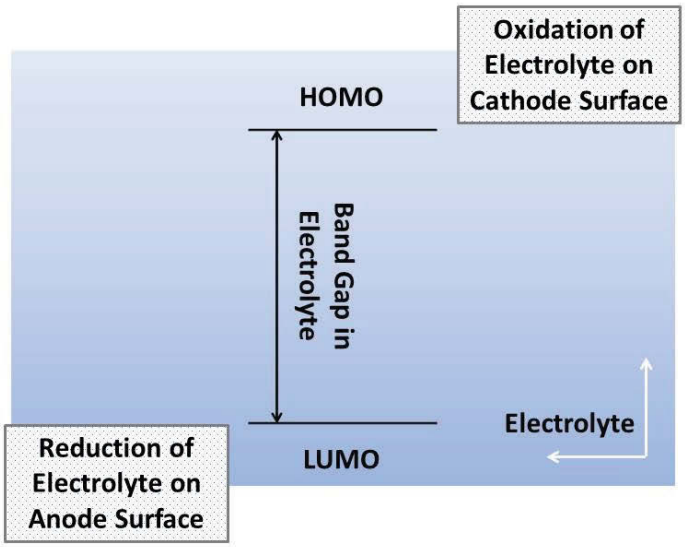

Figure 2.1 Schematic Illustration of Electrolyte Redox Reactions on Anode and Cathode Surfaces

High energy battery can be realized through two major approaches. One is to use electrode materials with higher energy density. Another is to increase the voltage difference between anode and cathode couples by using cathode material with much higher operating voltage versus Li^0/Li^+. In case of lithium batteries, the major difficulty in the application of high voltage cathode materials is the poor electrochemical stability of electrolytes (e.g. $LiPF_6$ in ethylene carbonate/diethyl carbonate mixed solution) at voltage above 4.5V, which is beyond the highest occupied molecular orbital (HOMO) of electrolyte. The high operating voltage of cathode leads to the electrolyte oxidation and the formation of passivation layer on the surface of cathode [6]. Thus cathode materials with high operating voltage versus Li^0/Li^+ commonly exhibit decreased capacity and low coulombic efficiency. Using electrolyte with wide electrochemical-stable window, or adding additives in electrolyte to suppress the oxidation process are possible ways to solve the problem [7]. However, the organic electrolyte with a wide electrochemical-stable window has yet been discovered, and the effects of electrolyte additives are also limited due to the reactivity of the high voltage cathode. Thus, the long term stability of high voltage LIB remains problematic.

Current cathode materials used in LIB have their own advantages and disadvantages, and therefore have different fields of applications. For example, the $LiCoO_2$ cathode with relatively higher capacity is widely used as the power sources in portable

electronics. However, the high production cost, high toxicity, as well as the chemical instability under deep charge prevent it from large scale applications. $LiMn_2O_4$ and olivine $LiFePO_4$ are better choice as cathode materials for BEV applications due to their low cost, low toxicity and excellent chemical stabilities at high current rate. However, the energy densities of $LiMn_2O_4$ and $LiFePO_4$ are less than that of $LiCoO_2$, which largely limits the energy storage capability of prospective battery systems.

From the above introduction of LIB components, it is easy to conclude that the modification of electrode and electrolyte materials is essential for the development of lithium battery with both high power and high energy densities. Nanostructured carbonaceous materials, metal oxide materials and metal sulfide materials are potential alternatives of current electrode materials in use for LIB due to their capabilities of delivering higher energy density. There are also groups of high capacity electrode materials such as lithium alloy anodes, sulfur and oxygen cathodes which operate based on mechanisms quite different from lithium insertion/removal also can be applied in the configuration of high energy lithium batteries [5].

2.2 Nanostructured Anode Materials

The deficiency of graphite anode materials largely limits the development of LIBs towards reliable energy storage system with high capacity and better reliability in the future. This fact has prompted interests in search for substitutes of graphite

anode. Potential substitutes of graphite anode include nanostructured carbon materials, lithium alloy-based anode materials, metal oxide anode materials, and metal sulfide anode materials.

2.2.1 Nanostructured Carbon Anode Materials

Nanostructured carbonaceous anode materials with potential of high degree of lithium intercalation reactions have been tested as anode materials to increase the energy density of lithium-ion batteries. One-dimensional nanostructured carbon anode materials (e.g. carbon nanotubes) and two-dimensional nanostructured carbon anode material (e.g. graphene) can offer higher capacity for lithium storage than graphite. The relatively high capacity of CNTs is attributed to delocalization effect of electrons within the nanotube structure which offers more electrochemical negativity than graphite. Two-dimensional graphene nanosheet has a superior surface area to volume ratio due to its unique honey comb lattice and one-atom thick monolayer structure. Its unique structure can provide large number of reaction sites for lithium storage. However, the low coulombic efficiencies and large irreversible capacities of CNTs and graphene nanosheets are the main drawbacks for their application as anode materials for LIB [8-10].

2.2.2 Nanostructured Lithium Alloy Anode

Lithium alloy anode materials have high operating voltages above that of Li^0/Li^+ as well as huge capacity values, which made them appealing candidates for high

energy lithium battery system. Metals and semiconductors such as aluminum, tin and silicon, can react with lithium electrochemically and form alloy. The allying/de-alloying process is partially reversible, involving a large number of atoms and electrons exchange per formula unit, hence provide large specific capacity. For example, the specific capacity of Li-Si anode is 3580mAh/g with a lithium ion saturation concentration of $Li_{3.75}Si$, and that of Li-Sn anode is 990mAh/g with a lithium ion saturation concentration of $Li_{4.4}Sn$. However, there are some problems of lithium alloy anodes which need to be solved before their fully utilization in LIB. The main drawback of lithium alloy anodes is the large volume change of anode during charge and discharge process. The continuous alloying and de-alloying mechanism exerts lattice stress and causes structural cracking of anode [11]. As a result, lithium alloy anodes have serious capacity loss within a few charge-discharge cycles. The solution to this particular issue is using binary composite with large free volume to buffer the volume change. In the typical binary composite model, with one component alloy/de-alloying with lithium while the other inactive component working as protective structure against the volume expansion, the structural stability of anode will be retained and the cell can sustain a long term cycle life. Many reported studies on lithium alloy based anode materials have corroborated the effectiveness of the above strategy [12-14].

2.2.3 Nanostructured Metal Oxides and Metal Sulfides

A variety of nanostructured metal oxide (MO) and metal sulfide (MS) anode

materials have been studied as alternatives of graphite anode [5, 7, 15]. Metal oxide anode materials, as a large group of compounds, are found have very different reaction mechanisms with lithium [16-18]. In general, there are three types of reactions can take place between lithium/metal-oxide couples, including lithium intercalation, lithium-metal alloying and lithium-metal conversion.

The lithium intercalation reaction of metal oxide anode involves the lithium ion insertion/removal of transition metal oxides. This type of reaction does not involve any phase changing of metal oxides, thus insertion based metal oxide anode materials can offer reliable performance such as good capacity reversibility, high rate capability. However, the insertion metal oxide anodes have the same problem as graphite anode in terms of energy density. Those insertion metal oxides usually have a small saturation of lithium concentration which leads to a theoretical capacity even less than that of graphite anode. For example, rutile titanium oxide (TiO_2) anode can exhibit high rate capability at voltage window from 1.0 V to 3.0 V (versus Li^0/Li^+) and excellent electrochemical stability upon cycling, but the rutile titanium oxide anode can only accommodate lithium up to a stoichiometry of $Li_{0.5}TiO_2$, which equivalent to a specific capacity of 168 mAh /g [19].

Another type of metal oxide anode works based on lithium-metal alloying mechanisms. During the lithium-metal alloying reactions, metal phase of metal

oxide anode reacts with lithium ions and form alloy. This type of MO anodes can generate large numbers of lithium/electron exchanges therefore have high theoretical capacities. For example, tin oxide (SnO_2) anode can react with lithium to generate Li_2O and Sn, and subsequently form Li-Sn alloy with a saturation lithium concentration of $Li_{4.4}Sn$ (See Eqn 2.1 and 2.2), which is equivalent to a theoretical capacity of 790 mAh/g (differs from that of Li-Sn alloy anode)[20].

$$SnO_2 + 4e + 4Li^+ \rightarrow 2Li_2O + Sn \quad (2.1)$$

$$Sn + 4.4e + 4.4Li^+ \rightarrow Li_{4.4}Sn \quad (2.2)$$

Compared with solid SnO_2 particles, porous SnO_2 nanostructures are better choice for anode materials due to their ability to buffer volume changes, but the high surface area of nanostructured porous SnO_2 also brings in the deficiency of irreversible capacity [21, 22]. However, the application of alloy based metal oxide anodes are inhibited by the large volume change of anode materials upon continuous cycling. The main challenge of alloy based metal oxide anodes remains maintaining the structure integrity during charge-discharge process.

The third type reaction mechanisms of metal oxide anode are conversion process. The conversion process between lithium and metal oxides refers to the electrochemical process during which metal oxides are converted to the metallic

state along with the formation lithium oxide (Li_2O) and returned to its initial state in the reversal reactions. This conversion reaction between metal oxides and lithium composes the formation and decomposition of lithium oxide and the reduction and oxidation of metal. The reaction mechanism of lithium/metal sulfide couples is the same as the conversion process of metal oxides, which can be described as follows [23]:

$$Mn^{+}X + ne^{-} + nLi^{+} \rightleftharpoons M^{0} + nLiX, (X = S, O) \quad (2.3)$$

Metal oxide/sulfide anode materials that react with lithium based on conversion mechanism offer high reversible capacities and high energy densities due to the large numbers of ion/electrons exchange involved in conversion reactions. Thus the conversion-based metal oxides or sulfides have the potential to develop high energy electrodes. However, those metal oxides/sulfides have problems such as low coulombic efficiency, large potential hysteresis, and low capacity retention rate over long cycles [24, 25].

Cobalt sulfides with high capacity and cycle stability are attractive anode materials for LIBs. The high initial capacity of 1280 mAh/g achieved from a CoS_2 anode from the preliminary study revealed the great potential of developing high energy storage systems with cobalt sulfides [26]. Cobalt sulfides with different

compositions and structures (Co_3S_4, CoS, Co_9S_8, and CoS_2) have been found applications in a broad field including semiconductor, chemical catalysts and magnetic materials [27-31]. Although many research groups have reported synthesis and corresponding electrochemical characterization of cobalt sulfides as anode materials [32-35], there are still more potential cobalt sulfides materials have not been investigated as anode materials. Tin sulfides are also potential anode materials with high capacity. Tin disulfide (SnS_2) was the first material in tin sulfides that has been examined as anode material [36]. SnS_2 nanoplate [37] , 3D-flower SnS_2 [38] and SnS_2/SnO_2 composite [39] along with other tin sulfides which possess different morphologies have been characterized for their electrochemical performance as anode materials [40-43]. So far, the capacity deterioration and irreversible discharge capacity at the first cycle are still the main issues for cobalt/tin sulfides anode materials remains.

Recent reported works on the synthesis of one-dimensional metal sulfides include copper and nickel sulfide cathodes, which may have created a path towards the performance improvement of metal sulfide electrode materials [44, 45]. Well-designed material morphology can contribute to the improvement on electrochemical performance of electrode materials. Those synthesized one-dimensional metal sulfide cathode materials exhibit capacity stability over prolonged charge-discharge cycles and, similar to carbon nanotubes, good rate

capability. However, the capacity fading of those metal sulfide cathode after the first cycle discharge remains high, in comparison with the same materials with higher dimensional structure.

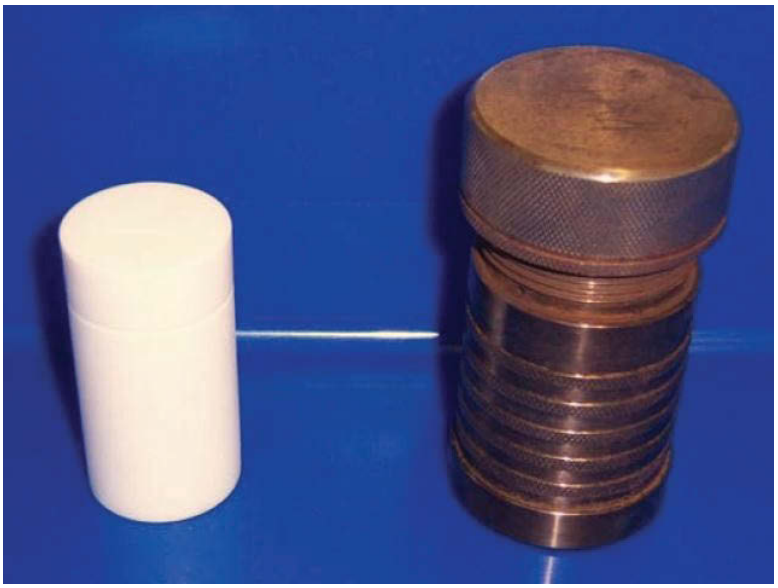

Figure 2.2 Reactors for hydrothermal synthesis: teflon-lined autoclave (left) and stainless steel container (right).

Hydrothermal synthesis is a common synthesis method for nanostructured material preparation due to its high efficiency in producing nanostructure materials [46-50]. The solvent for hydrothermal synthesis are widely available, and the reaction process with organic solvents is often referred as solvothermal synthesis. The reactions of hydrothermal synthesis are carried under high pressure, high temperature solution environment. This method utilizes the solubility of materials in prospective solvents under high temperatures, high pressures conditions and

subsequent crystallization of the dissolved material from the solution. The changes of properties of solvents and reactants at high temperatures and high pressures provide more favorable condition to produce materials with complex nanostructures, which are difficult to achieve at normal environment. Another key feature of hydrothermal synthesis is that the desirable simultaneous nucleation rate and good size distribution, which are important to the morphology and performance of nanostructure materials, can be obtained by controlling reaction parameters such as pressure, temperature, reaction time.

Nano-structured metal oxide/sulfide materials are potential high energy electrode materials for LIBs. But the involvement of nanoscale structure in electrode synthesis has both opportunities and challenges. The modification of material morphology at nano meter scale can offer a variety of advantages, including large surface area to volume ratio and shortened path for electronic transfer and ionic diffusion. High surface area of electrode materials can improve the capacity and rate capability of electrode materials due to the increase of large electrode/electrolyte contact area and increased degree of lithium intercalation. Shortened path for electronic transfer and ionic diffusion lead to low electronic and ionic resistance, which is good for the application of electrode materials with poor conductivity. On the other hand, the use of nanostructured electrode materials may also leads to negative effects such as the decrease of battery energy densities and coulombic efficiency. The decreased

battery energy densities are mainly caused by the large free volume within the nanostructured electrode material. The high surface area of nanostructured electrodes causes increase of undesirable side reactions at electrode-electrolyte interface. Those side reactions of electrode/electrolyte species can leads to a series of defects such as irreversible capacity, low coulombic efficiency, poor cycle stability or safety hazards of lithium batteries. In addition, the material synthesis of nanostructured electrodes is difficult due to the requirement of controlling the particle shape, size and size distribution. Structure defects can also be generated because of the complexity of synthesis mechanisms.

2.3 High Energy Cathode Materials

Innovative configurations of rechargeable lithium batteries such as lithium-air battery and lithium battery represent the evolved battery chemistry of lithium battery. With redox reactions between lithium and oxygen/sulfur, those batteries offer much higher energy storage capabilities compared with LIBs.

Lithium-Air battery (Li-Air battery) with the redox couple of lithium metal (anode) and oxygen (cathode) offers a theoretical specific energy of 11,680 Wh/kg. With proper electrolytes, the lithium-oxygen redox reaction can be reversed therefore forming a reversible charge-discharge mechanism. Li-Air battery is considered the only power source that may be on a par with gasoline in terms of usable energy

density. However, due to the absence of feasible solution that can maintain oxygen contact with lithium while isolating the undesirable contamination from air, the realization of practical Li-Air battery is currently inhibited by a series of technique issues including cost, power, energy density, lifetime, and cycle stability [51].

Lithium-Sulfur battery (Li-S battery) works on the basis of redox reactions between lithium metal anode and sulfur cathode. The reaction in Li-S battery is a reversible conversion reaction. Sulfur cathode offers a theoretical capacity of 1672 mAh/g and a theoretical energy density of 2600 Wh/kg with the fully utilization of sulfur in the following process:

$$16Li^{+} + S_8 + 16e^{-} \rightleftharpoons 8Li_2S \qquad (2.4)$$

Thus sulfur cathode in a Li-S battery system has the highest theoretical capacity value of all known solid state cathode materials. Li-S battery has the great potential as high energy power source for wide ranges of applications due to its high theoretical capacity, intrinsic overcharge protection mechanism, elemental abundance, low cost and nontoxicity [52]. However, the utilization of sulfur cathode has the challenge related to increasing active mass utilization rate, suppressing the capacity fading over long cycle life and constraining the safety hazards of the lithium metal anode. The development of Li-S battery is inhibited by its severe capacity

deterioration, which is mainly caused by the high solubility of sulfur in organic electrolyte.

2.3.1 Discharge Mechanisms of Sulfur Cathode

The discharge reaction of sulfur generates various forms of intermediate polysulfides in both the electrolyte phase and the sulfur electrode phase due to stepwise reduction processes. There are mainly two stages of the discharge reaction of sulfur cathode:

$$S_8 + Li^+ + e^- \rightarrow Li_2S_x \text{ (first discharge stage, 2.4 V – 2.1 V)} \quad (2.5)$$

$$Li_2S_x + Li^+ + e^- \rightarrow Li_2S_2 \text{ and/or } Li_2S \text{ (second discharge stage, below 2.1 V)} \quad (2.6)$$

The first discharge region attributes to the dissolution of solid sulfur and formation of high order polysulfides (Li2Sx, X>3). Those high order soluble polysulfides can migrate towards lithium anode through electrolyte. As the discharge process continues, the low order, insoluble polysulfides (Li2Sx, $X \leq 2$) accumulate at cathode surface in the second discharge region and lead to an irreversible capacity [53, 54]. The sulfur dissolution in organic solvents may also causes self-discharge behavior of Li-S battery [55]. An average daily capacity loss of 3% is reported in TEGDME based electrolyte with aluminum current collector. The capacity loss with stainless steel current collector is much more serious due to the electrochemical corrosion [56,

57].

2.3.2 Electrolyte for Li-S battery

The high solubility of sulfur and formation of polysulfides dictate that electrolytes used for LIB are no longer suitable for Li-S battery. Generally, the requirements for the electrolyte served in Li-S battery include high ionic conductivity, high electrochemical stability with polysulfides and low viscosity. A number of studies have been reported on the effect of electrolyte component, including tetrahydrofuran (THF), 1,2-dimethoxyethane (DME), 1,3-dioxolane (DOX), tetra(ethylene glycol)dimethyl ether (TEGDME), to the capacitance and cycle performance of Li-S battery[55, 56, 58-77]. It seems rather difficult for any single organic solvent to satisfy all those conditions of Li-S battery electrolyte. A practical solution is to use electrolyte with the optimized formula based on a mixture of solvents and additives. Ether type solvent has a good solubility of sulfur while maintaining electrochemical stability of polysulfide, and cyclic solvent can contribute to the stabilization of lithium anode surface. Mixed solvents consist of both ether solvent and cyclic solvent can achieve the dynamic balance between the sulfur dissolution and chemical stability of electrolyte against lithium metal. Tetra(ethylene glycol)dimethyl ether (TEGDME)/ 1,3-dioxolane (DOX) and Diethylene glycol dimethyl ether (Diglyme)/1,3-dioxolane (DOX) are attractive organic solvent mixture for sulfur cathode due to its ability to deliver first discharge capacity of over 1200 mAh/g (based on sulfur content in cathode) [72]. The solvent

combination of 1, 2-dimethoxyethane (DME) and 1,3-dioxolane (DOX) has also been corroborated good electrolyte solvents which can greatly improve the overall performance of Li-S battery [78, 79]. The DME controls sulfur solubility and the electrochemical reaction of polysulfides while DOX acting as stabilizer of polysulfides in electrolyte against lithium metal [62]. DOX and $LiN(SO_2CF_3)_2$ (LiTFSI) salt are found playing important roles in reactions which lead to the formation of protective film comprising Li_xNO_y and/or Li_xSO_y on lithium anode surface [80].

The applications of polymer electrolyte and ionic liquid electrolyte in lithium-sulfur system have also been explored. A few studies demonstrated the application of ionic liquid electrolytes in Li-S battery [68, 77]. Ionic liquids can improve the cycle performance of sulfur cathode by suppressing polysulfides dissolution in electrolyte phase. The good chemical and thermal stability of ionic liquid also help increase the safety of battery applications. However, the revealed results are insufficient to verify the effectiveness ionic liquid electrolyte in Li-S battery due to their limited charge-discharge cycles. The solid state battery configuration may help overcome those problems related to sulfur and dissolution. The major improve from the polymer electrolyte is using solvent-containing polymer membrane to avoid direct contact between electrode and organic solvents. Hence solid state Li-S battery can be expected to have improved reliability and safety. There are a few Li-S battery with poly (ethylene oxide) (PEO) based polymer electrolytes have been investigated

and some Li-S battery with imbedded polymer electrolyte have demonstrated relatively good cycle performance [62-65, 81-83]. However, the polymer electrolytes have weak spot on its temperature-dependent performance. Lithium diffusion through PEO-based electrolytes mainly occurs in amorphous regions of polymer which requires high ambient temperature. PEO based polymer electrolyte can achieve full sulfur utilization at the temperature of 90°C for the initial discharge, but polymer crystallization and electrolyte polarization at lower temperature leads to incomplete reactions of sulfur due to poor electrochemical contact of cathode and electrolyte [64, 83].

2.3.3 Morphology of Sulfur Cathode

The electrical and ionic insulating nature of sulfur results in a low level active material utilization of sulfur cathode. The sulfur content in cathode may not be fully discharged or charged due to poor electrochemical contact within the electrode material. It is necessary to add additives with high conductivity to form binary or ternary composite sulfur cathode in order to improve the electrical and ionic conductivity of sulfur content. The common solution is to synthesize carbon-sulfur composite cathode, in which carbon matrix can provide both electron transport network and reaction sites for lithium-sulfur redox reactions. Chemical-free process such as melt-diffusion and ball-milling techniques are commonly used to prepare composite sulfur cathode materials with relatively simple morphologies. The melt-diffusion strategy refers to a thermal process for preparation of carbon/sulfur

composite material, during with the solid sulfur was heated to a liquid state and return to solid state while attached to conductive agents. By heating the carbon/sulfur mixture to a temperature above the melting point of sulfur, liquid sulfur with low viscosity can easily flow into inner spaces of carbon matrix. Infiltrating sulfur into carbon matrix through melt-diffusion has been proved an effective approach to enhance the performance of sulfur cathode. Many carbonaceous materials with different morphology and structure such as carbon nanotube, porous carbon and graphene have been used for synthesis of sulfur composite cathode materials. Ball-milling, as a mechanical processing method widely adopted for the preparation of powder productions, can also be used for sulfur cathode preparation. During the milling process, the stainless balls (or other grinding media) rotate around a horizontal axis in a tumbler, partially filled with the sulfur mixture. The continuous rotate press can reduce the size of bulk particles within sulfur mixture and generate fine powders. Considering the fire risk due to the flammable nature of sulfur and possible sparks generated form the collision of steel balls and the tumbler, the ball milling preparation of sulfur cathode are usually conducted with inert gas protection. The sulfur cathode material prepared with ball-milling method can achieve a relatively good distribution of sulfur particles with average size from 3μm to 8 μm [53], which largely limits its range of applications in conductive materials with smaller pore sizes.

Multi-wall carbon nanotubes (MWCNTs) have been applied for synthesis of binary and ternary sulfur cathode materials [69, 84-87]. As a conductive agent with good mechanical strength and chemical stability, carbon nanotubes can provide a good electrical path for the redox electrochemical reaction sites for sulfur in the composite. The configuration of CNTs/sulfur cathode can be divided into three major groups: (1) bulk sulfur particles enwrapped by carbon nanotubes, (2) core (MWCNTs)/shell (sulfur) structure composite and (3) a blend of sulfur particles and MWCNTs in polymer. The carbon nanotubes can provide more effective electronically conductive networks within the composite compared with amorphous carbon additives. Highly conductive networks in the sulfur cathode via homogeneous dispersion of carbon nanotubes (CNTs) can greatly improve the rate capability and the cycle stability of Li-S battery [84]. However, the structural properties of CNTs, such as diameter, length, surface area and pore volume, largely limit the room for further improvement on the performance, especially the specific capacity, of MWCNTs/sulfur composite due to the limited capacity of sulfur load on carbon nanotubes.

Porous carbon with highly ordered porous structure and interconnected channels exhibits high pore volume, uniform pore size distribution, and high conductivity. The existence of micro carbon fibers within mesoporous carbon provides both electrochemical contact and strong support of nano-architecture [88, 89]. The

structural properties of mesoporous carbon (pore sizes 2 nm to 50 nm) have attracted attention for its application in functional materials including sulfur cathodes [77, 81, 90-93]. The conversion process between sulfur and lithium during charge and discharge leads to the volume change of both lithium anode and sulfur cathode [94]. By trapping sulfur into porous carbon, the free volume of carbon matrix can provide buffer for the expansion and contraction of sulfur content, which can contribute to the improvement of the cycle stability. Some research groups have demonstrated porous or core(sulfur)/shell(porous carbon) structure carbon/sulfur composites based on similar concept and achieved preferable sulfur utilization rates [76, 95-97].

Graphene, with its good properties such as high conductivity, chemical stability, mechanical strength, and large surface area, has been intensively studied for electrochemical energy storage applications from super capacitors to lithium-air battery [98-109]. Graphene sulfur composites are considered as new approaches to improve the performance of Li-S battery. The excellent electrical conductivity of graphene ensures good electrical contact between adjacent sulfur particles. The mechanical flexibility of graphene offers sulfur composites with sandwich-type or wrapping-type architectures which accommodate the volume change of the sulfur during charge-discharge process. Hence, the graphene-sulfur cathodes showed relatively good sulfur utilization rate in Li-S battery [110-112].

Table 2.1 listed a series of sulfur cathode synthesized from various physical - chemical processes. Although some of reported sulfur cathodes have achieved high specific capacity over 1000 mAh/g or high rate capability up to 7 C (equivalent to 11,700 mA/g) [70, 87, 92, 95, 112], it is still difficult of retain the high and stable capacity of sulfur over 100 cycles. The reported sulfur cathodes synthesis mainly focused on the structure characteristics of carbonaceous materials and lack of control measures on the particle size of solid state sulfur, the size distribution of sulfur within the cathode is commonly neglected. To the best of my knowledge, the modification of particle size of solid sulfur at electrode material synthesis stage has yet to be investigated in previous research works.

Table 2.1 Performance of Sulfur Cathodes with Different Components

Conductive Content In Cathode	Electrolyte	Initial Capacity	Charge-discharge Cycles	Remained Capacity
Polyacrylonitrile[97]	$LiPF_6$ in EC/DMC	~500 mAh/g	380	470 mAh/g
poly(pyrrole-co-aniline)[113]	$LiCF_3SO_3$ in DME/DOX	1285 mAh/g	40	866 mAh/g
MWCNTs[85]	$LiCF_3SO_3$ in DGDE /DOX	1380 mAh/g	30	1020 mAh/g
Amorphous Carbon[96]	$LiClO_4$ in DGDE/DOX	1232 mAh/g	50	>800 mAh/g
Mesoporous Carbon[114]	$LiPF_6$ in EMS	1320 mAh/g	20	>800 mAh/g
Porous Hollow Carbon[93]	LiTFSI in Tetraglyme	1071 mAh/g	100	974 mAh/g

Overall, LIB is reaching its limits in performance with current electrode and electrolyte materials. Breakthroughs in materials and battery chemistry are essential to expand battery applications in the future. Solutions to above difficulties may include but not limit to the application of nanostructured electrode materials in LIBs, innovation of battery chemistry and development of rechargeable lithium batteries with different working principles. Lithium-sulfur battery with lithium and sulfur redox couples offers highest theoretical capacity among all known solid state cathode materials. High energy density, elemental abundance, low cost and low toxicity of sulfur guarantees the great potential of lithium-sulfur battery as high energy power source and alternative for lithium-ion battery.

3 Experimental Design

In this research project, I mainly focused on the correlations between sulfur particles size and the performance of sulfur cathode. An innovative synthesis of sulfur cathode through sonication was conducted in order to achieve reduced size of sulfur particles. The morphology of carbonaceous material was also investigated as a variable to sulfur cathode performance. The research methodology I used for this project mainly includes the electrochemical performance analysis (i.e. cyclic voltammetry, electrochemical impedance spectra and charge-discharge cycle tests) and material characterizations techniques (i.e. x-ray diffraction, scanning electron microscope, thermal-gravimetric analysis). Experiment works are divided into four stages in terms of content. The first stage is the synthesis of materials. There are mainly three types of sulfur cathode materials investigated in this research project. Those cathode materials include amorphous carbon/sulfur cathode, mesoporous carbon/sulfur cathode and graphene/sulfur cathode. The second stage is material characterization. The experiment works in this stage are mainly examination of variety characteristics of synthesized materials, including material morphology, structure and mass ratio of different component in those materials. The third stage includes electrode fabrication and battery assembling, where electrode materials are assembled as coin cells with lithium as counter electrode for further electrochemical characterization. The effect of different electrode fabrication technique on the battery performance is also one of many research objectives. The

last stage is electrochemical test of lithium batteries. The test techniques are common electrochemical analysis measures such as cyclic voltammetry tests, electrochemical impedance tests and galvanostatic charge-discharge tests.

3.1 Material Synthesis

The materials synthesized in this research project include graphene nanosheets, graphene/sulfur composite, rod-shape mesoporous carbon and amorphous carbon/sulfur composite. The synthesis techniques of sulfur containing composites include solvent assisted synthesis and melt-diffusion synthesis. The solvent assisted synthesis method is using the organic solvent to dissolve sulfur than create composite of sulfur and carbon materials through the formation of precipitate. Melt-diffusion synthesis refers to the thermal treatment of carbon /sulfur mixture.

3.1.1 Chemicals Used In Materials Synthesis

The chemicals involved in this research project are listed in Table 3.1. Table 3.1 listed the major chemicals I used for synthesis of sulfur cathode with different morphologies. All solid chemicals are used as received without further purification.

Table 3.1 List of chemicals used for sulfur cathode material synthesis

Chemical Name	Formula	Purity/Concentration	Supplier
Sulfur	S	analytical-reagent	Sigma-Aldrich
Graphite	C	n/a	Bay Carbon
Hydrazine monohydrate	$NH_2NH_2 \cdot H_2O$	98%	Sigma-Aldrich
Potassium permanganate	$KMnO_4$	≥ 99.0%	Sigma-Aldrich
Sodium nitrate	$NaNO_3$	≥ 99.0%	Sigma-Aldrich
Sulfuric acid	H_2SO_4	> 95%	n/a
Dimethyl sulfoxide	$(CH_3)_2SO$	≥ 99.5%	Sigma-Aldrich
Carbon disulfide	CS_2	≥ 99.9%	Sigma-Aldrich
Carbon black	C	n/a	Vulcan
Sucrose	$C_{12}H_{22}O_{11}$	99.5%	Sigma-Aldrich
Hydrochloric acid	HCl	2mol/L	n/a
P123	$PEO_{20}PPO_{70}PEO_{20}$	bio-reagent	Sigma-Aldrich
Ethanol	CH_3CH_2OH	99%	n/a
Tetraethyl orthosilicate	$Si(OC_2H_5)_4$	98%	Sigma-Aldrich

3.1.2 Melt-Diffusion Technique

The melt-diffusion method utilizes the transformation from solid state sulfur to liquid state with the change of temperature. Liquid sulfur with low viscosity can easily flow into inner spaces of a porous structure and form composite. Sublimed sulfur and a structural material are two basic components for this synthesis process. The requirements for suitable structural material include inner free volume and structural stability at the temperature range above the melting point of sulfur. The materials used as structural support can be carbonaceous materials, polymers or ceramics. With the easily established procedure and low cost, this method can be applied to almost all kinds of carbonaceous materials. However, the morphologies of melt-diffusion synthesized sulfur composite materials and their performance as cathode materials are highly dependent on the properties of structural materials. In this research, I applied melt-diffusion technique to synthesis sulfur composites with graphene and mesoporous carbon. The detailed synthesis procedures are given in Chapter 4 and Chapter 7.

3.1.3 Solution Based Synthesis

The solvent carbon disulfide (CS_2) has a high solubility of sulfur at room temperature and a low boiling point of 46.3 °C. The observation in a series of trial experiments on sulfur dissolution in pure CS_2 solvent confirmed that (1) 4 – 8 g sublimed sulfur powders were fully dissolve in 20 ml CS_2 solvent at room

temperature and formed colorless solution, (2) amorphous sulfur precipitate formed from recrystallization after the CS_2 solvent fully vaporized. Due to the high sulfur solubility in CS_2 solvent, the reaction window for sonication on sulfur particles in sulfur - carbon disulfide solution is very small and the experiment parameters are hard to control. Thus the sonication technique is impractical in CS_2 solvent. I conducted solution-route synthesis with CS_2 solvent to synthesis sulfur composite with amorphous carbon. The detailed synthesis procedures are given in chapter 5.

3.1.4 Sonication Technique

Ultrasound process is the method of choice to synthesize sulfur/carbon composite through a solution route with dimethyl sulfoxide as the solvent. Ultrasound has been employed in a wide range of chemical applications including dispersion of powdered solids in a solid-liquid system due to its high efficiency in reaction rates [115]. Because ultrasonic shock waves from cavitation collapse can produce large forces on small particles [116], the fragmented sulfur after sonication process is expected to have a relatively small size and increased surface area. Hence the electrochemical conductivity within the cathode can be improved with reduced particle size and homogeneous size distribution of sulfur. The thermal effect of ultrasonic probe in liquid environment also makes it the perfect energy source for sulfur/carbon composite synthesis.

Dimethyl sulfoxide (DMSO) is a solvent with a high boiling point of 189 °C and a high

freezing point of 18.5 °C. The solubility of sulfur in DMSO is relatively high at the temperature above 115 °C. The observation in a series of trial experiments confirmed that (1) 2 – 4 g sublimed sulfur powders were fully dissolve in 50 ml DMSO solvent at temperature above 115 °C and formed solution with light yellow color, (2) needle-shape sulfur precipitate formed from re-crystallization after the solution cooled to room temperature. Thus the dissolution process of sulfur in dimethyl sulfoxide can be tuned by controlling the temperature of sulfur/DMSO solution. I conducted sonication synthesis technique which utilizes the DMSO solvent to synthesis sulfur nanocomposite with amorphous carbon. The detailed synthesis procedures are given in Chapter 6.

3.2 Materials Characterization

The techniques I used for material characterization include X-ray diffraction (XRD), scanning electron microscope (SEM) and thermal-gravimetric analysis (TGA).

3.2.1 X-Ray Diffraction

X-Ray Diffraction (or X-ray diffractometry, XRD) is a characterization technique widely used in materials science. Its applications include qualitative phase identification, quantitative phase analysis, determination of crystal structure, particle size and strain measurements, etc.

X-ray is a form of electromagnetic radiation with high energy and short wave length.

As the distance between atoms is on the same order as X-ray wavelengths, crystals can diffract the x-ray radiation when the diffracted beams are in-phase. For a given wavelength, diffraction can only occur at a certain angle with a fixed distance between atomic planes.

X-ray diffractometer, as the primary instrument for XRD test, consist of three basic components: an X-ray tube, a sample holder, and an X-ray detector. X-rays are generated in a cathode ray tube (CRT) by heating a filament to produce electrons, accelerating the electrons toward a target by applying a voltage, and bombarding the target material with electrons. The high energy electron beam will knock core electrons out of atoms and create vacancies. As electrons from a higher energy level make a transition to fill the vacancies, the characteristic x-ray emission is therefore formed. The characteristic X-ray spectra consist of several components, the most common being K_α and K_β. K_α consists of $K_{\alpha1}$ and $K_{\alpha2}$. $K_{\alpha1}$ has a slightly shorter wavelength and twice the intensity as $K_{\alpha2}$. $K_{\alpha1}$ and $K_{\alpha2}$ are close in wavelength so a compositive K_α is often used for XRD. Copper is the most common target material for X-ray diffraction and generates Cu-K_α radiation with a wavelength of 1.5418Å.

During the X-ray diffraction test, X-ray beam is directed to the sample. The sample rotates in the path of X-ray beam at an angle θ while the X-ray detector is mounted on an arm to collect the diffracted X-rays and rotates at an angle of 2θ. For typical

powder samples, a 2θ range of 5° to 70° degrees is sufficient to cover the most useful part of the powder patterns. As the sample and detector are rotating, the intensity of the reflected X-rays is recorded. When the geometry of the incident X-rays impinging the sample satisfies the Bragg Equation, constructive interference occurs and a peak in intensity occurs. The recorded X-ray signal is then transferred to a connected computer for data processing.

The XRD examinations of the obtained materials were performed on a Siemens D5000 X-ray diffractometer with Cu-K_α radiation. The scan angle I used was between 10° and 90° (or 10° to 80°), and the scan rate was 1° per minute.

3.2.2 Scanning Electron Microscope

The scanning electron microscope (SEM) is a technique used to investigate the structural properties of materials with interactions between high energy electrons and samples. The principle of SEM is using a focused beam of high energy electrons to generate a variety of signals at the surface of solid specimens. The signals that derive from electron-sample interactions (as shown in Figure 3.1) can be used to reveal information about the sample's morphology. The SEM is capable of performing analysis of selected point locations on the sample. In most cases, data are collected over a relatively small area (1 cm to 10 micron in width) on the surface of the sample, thus a series of images that displays detailed information of sample properties can be acquired. With properly selected detectors, SEM can also be used

for revealing qualitative information of samples such as chemical compositions, crystalline structure, and crystal orientations.

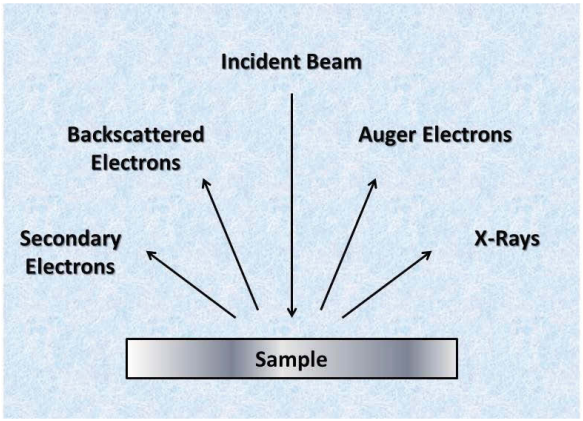

Figure 3.1 Schematic Illustration of Electron/Sample Interaction in SEM

Accelerated electrons in an SEM carry significant amounts of kinetic energy, and this energy is dissipated as a variety of signals produced by electron-sample interactions when the incident electrons hit the solid sample. These signals include secondary electrons, (diffracted) backscattered electrons, and photons etc. Secondary electrons and backscattered electrons are commonly used for imaging samples: secondary electrons are signal sources for displaying morphology and topography of samples, and backscattered electrons are signal sources for illustrating contrasts in composition in multiphase samples. X-ray generation is produced by inelastic collisions of the incident electrons with electrons in discrete orbitals (shells) of atoms in the sample. As those high energy electrons fall into lower energy states,

they yield X-rays with a characteristic wavelength. Thus, characteristic X-rays are produced for each element in a sample that is bombarded by the electron beam. The energy-dispersive (EDS) detector can be used to separate the characteristic x-rays of different elements into an energy spectrum, and the analysis the energy spectrum can be used to determine the abundance of specific elements in the sample. EDS can be used to find the chemical composition of materials down to a spot size of a few microns, and to create element composition maps over a much broader area.

During the interactions between incident electrons and sample, larger atoms (those with a higher atomic numbers) have a higher probability of producing elastic collisions because of their greater cross-sectional areas. Consequently, the number of backscattered electrons (BSE) reaching the BSE detector is proportional to the mean atomic number of the sample. Thus, highlight areas in backscattering image correlate with greater average atomic numbers in the sample, and dark areas in backscattering image have lower average atomic numbers. Backscattering images are very helpful for obtaining high resolution compositional maps of a sample and for quickly distinguishing different phases in a sample.

SEM utilizes vacuum conditions and uses electrons to form images, thus the sample preparations have a high standard in comparison with other material

characterization techniques. The sample for SEM must be water-free to avoid the water vaporization in the vacuum chamber. Samples with poor electronic conductivities need to be coated with ultrathin conductive layer (carbon or gold) on their surface. The coating process uses a small vacuum chamber (argon gas is also required for gold coating) along with an electric field.

General morphologies of materials and electrode surface were observed on a Zeiss Supra 55VP field emission scanning electron microscope. Back-scattering imaging and energy dispersive X-ray elemental mapping were also used to investigate the element distribution of sulfur nano-composite materials. I also used carbon coating on sulfur composite samples in order to obtain high quality images.

3.2.3 Thermogravimetric Analysis

Thermogravimetric analysis (TGA) is a technique used to determine changes in weight of samples in relation to the temperature variation. This result of TGA is dependent on accurate measurements of samples' weight and temperature. TGA is commonly employed in research to determine characteristics of materials such as degradation temperatures of materials, absorbed moisture content or solvent residua in materials, and the level of inorganic and organic components in materials. In this research, TGA is used to determine the composition of synthesized sulfur composite, i.e. the mass ratio of sulfur.

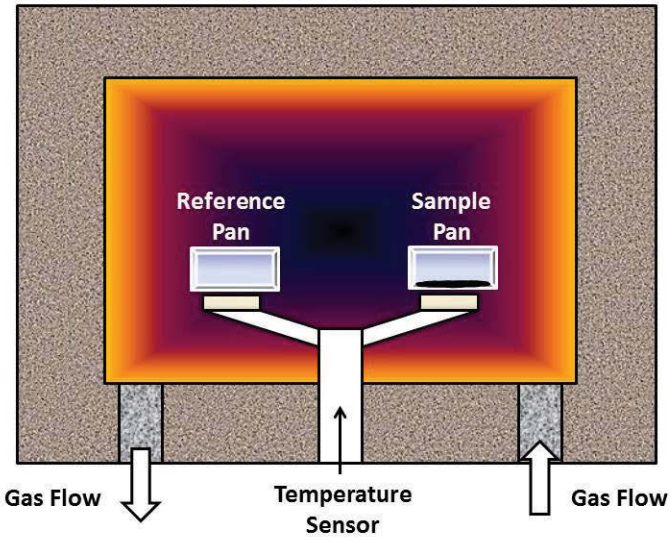

Figure 3.2 Schematic Illustration of Thermogravimetric Analysis

Figure 3.2 is the schematic illustration of thermogravimetric tester. The thermogravimetric analysis is conducted on a TA Instruments SDT 2960 TG/DTA analyzer. The weight of samples used in the analysis was 5 - 10 mg. The sample was first transferred into pre-balanced platinum open pan. Afterwards the sample pan along with reference pan was both transferred into the heating chamber. The experiment parameters were input into the control program as follows: (1) heating rate of 10 °C per minute, (2) temperature upper limit of 500 °C, (3) air atmosphere. The TGA results are converted to weight changes in a sample as a function of temperature.

3.3 Electrode Fabrication and Battery Assembling

There are two major methods for laboratory electrode fabrications: doctor-blade technique and roll-pressing technique. The doctor-blade coating technique is using vertical spatula to control the thickness of electrode film on substrate with the distance between the blade tip and substrate. The electrode paste can form a coating on substrate through the movement of blade on substrate surface. Roll-pressing technique is based on similar concept, only the vertical blade is replaced by a cylinder. In roll-pressing method, the electrode paste is coated on the substrate with the rotation of cylinder. The thickness of electrode film is controlled by the holder of cylinder.

Those sulfur cathodes I prepared for electrochemical tests are according to the following procedure. A blend of synthesized sulfur composite material (80 wt%), carbon black (10 wt%), and polyvinylidene fluoride (PVDF, 10 wt%) was mixed with N-methyl-2-pyrrolidone (NMP) to form a slurry. The slurry was then coated on aluminum foils. The coated aluminum foils were then transferred into a vacuum oven, dried at 80 °C for 12 h. After the bake-out, the coated aluminum foils were cut into round disks with a diameter of 14 mm and pressed with molds to form a compact layer of active mass.

As to the test battery assembling, lithium foils were used as the negative electrode. Test batteries were assembled as type CR2032 coin cells. The electrolyte used for Li-S battery tests was 1 mol/L lithium bis(trifluoromethane sulfone) imide (LiTFSI, $LiN(SO_2CF_3)_2$) salt in a mixed solvents of 1,2-dimethoxyethane (DME) and 1,3-dioxolane (DOX) (4:1 in volume ratio). The preparation of electrolyte and battery assembling were conducted in argon filled glove-boxes (Unilab, MBraun, Germany) with both moisture and oxygen levels below 0.1 ppm.

3.4 Electrochemical Testing

The test techniques are common electrochemical analysis measures such as cyclic voltammetry, electrochemical impedance spectroscopy and galvanostatic charge-discharge tests. Cyclic voltammetry is the most widely used technique to acquire qualitative information about electrochemical reactions such as the equilibrium of electrochemical reaction.

The $LiN(SO_2CF_3)_2$ salt I used to prepare the electrolyte for sulfur cathode tests is known as one of the most reactive salts and may cause corrosion of aluminum current collector (substrate of sulfur cathodes) in organic solvent electrolytes at the potential over 3.5 V (versus Li^0/Li^+). Thus, I conducted all electrochemical tests within the voltage window between 1.0 V and 3.0 V in order to avoid undesirable side reactions between electrolyte and aluminum current collector.

3.4.1 Cyclic Voltammetry

Cyclic voltammetry (CV) is a widely used technique for acquiring qualitative information about electrochemical reactions of batteries. It offers a rapid location of redox potentials of the electrode/electrolyte species.

During the cyclic voltammetry test, a series of voltages are applied to the battery at a constant rate (e.g. 1mV/s) and fixed voltage range (e.g. 1.0 V - 3.0 V). The voltage is swept back and forth between the upper limit and lower limit and the corresponding currents are monitored. The received current response is plotted as a function of voltage.

A CV scan starts with zero current flow. As the voltage is swept further to the reductive (or oxidative) region, a current flow begins to form and eventually reaches a peak and then starts to drop. The peak area of current/voltage current indicates a high rate electron transfer in comparison with the voltage sweep rate. This principle can be used to determine the potentials of electrochemical reactions within a test cell.

The results of CV tests are highly dependent on a few factors including the voltage scan rate, the reactivity of the electrode/electrolyte species, and the rate of the electron transfer reactions. The rate of electron transfer can be influenced by the

applied voltage. Variable voltages applied on electrode can cause the change of the electrons' energy state and influence the activation energy of chemical species. The rate constants for the electron transfer are proportional to the exponential of the applied voltage. Therefore, as the voltage is changed, the reaction rate and the current will change exponentially. In a slow voltage scan the mass diffusion layer will grow much further from the electrode in comparison to a fast scan. Consequently the flux to the electrode surface is considerably smaller at slow scan rates than it is at faster rates. As the current is proportional to the flux towards the electrode, the magnitude of the current will be lower at slow scan rates and higher at high rates. The position of the current peak is a characteristic of electrode reactions which have rapid electron transfer kinetics. These rapid processes are referred to as reversible electron transfer reactions.

I conducted cyclic voltammetry measurements on CHI Electrochemical Workstations (CHI CJ660D) at a sweep rate of 0.1 mV /s in a potential range between 1.0 V and 3.0 V.

3.4.2 Electrochemical Impedance

The measurement of impedance of electrochemical interface has been applied to many fields including studies of metal corrosion behavior, development of solid

state electrolytes, charge state prediction of batteries, and material characterization of porous electrode.

In the electrochemical impedance measurement, the test battery is considered as a parallel circuit which consists of a capacitance (Cp) and an ohmic resistance (Rp). The relationship between current and applied voltage of a circuit can be characterized by the amplitudes of current, the voltage, and the phase shift. These quantities can also be represented as a complex number, thus the impedance response is usually characterized by a real part-imaginary couple. The data from impedance measurement is plotted as a complex plane with the frequency as a parameter. With a complex plane plot, the results are easy to be compared with the linearized model (parallel circuit).

The measurement of impedance is often carried with a frequency response analyzer. The capacitance and large time constant involved in electrochemical process dictate that the measurement of impedance has to be applied in a very wide frequency range (e.g. from 100 kHz to 0.001 Hz). The impedance changes between its high-frequency limit and low-frequency limit. The high-frequency limit refers to the contact resistance, and the low-frequency limit refers to polarization resistance.

The electrochemical impedance measurements I conducted were performed with CHI Electrochemical Workstations (CHI CJ660D) on assembled batteries at open potential. The frequency range was between 100 kHz and 0.01 Hz with the amplitude of 5 mV.

3.4.3 Galvanostatic Charge-Discharge Tests

The galvanostatic charge-discharge tests are conducted to evaluate the main performance index of Li-S battery, i.e. the specific capacity of sulfur content in synthesized composite materials, capacity retention rate and energy efficiency (coulombic efficiency). The voltage-capacity (V/Q) curves generated from charge-discharge cycle tests can also be used to elucidate electrochemical reduction/oxidation mechanisms of the cathode material. The charge/discharge cycling tests were performed on a Neware RS-232 battery test system in galvanostatic mode with cut-off voltages of 1.0 V and 3.0 V. Different current rates were applied on assembled Li-S battery in order to investigate the rate capability of sulfur cathodes.

All specific capacity data of tested electrode are based on the sulfur weight in electrode unless specified otherwise. The specific capacities of sulfur in tested batteries are calculated according to the following equations:

$$Q_{sc} = Q / W_s \quad (3.1)$$

$$W_s = (W_P - W_0) \bullet R_s \quad (3.2)$$

Where the Q_{sc} refers to the specific capacity of sulfur within the cathode, Q is the discharge (or charge capacity) capacity acquired from the monitor software of cycle tests, W_s is the amount sulfur mass of particular tested cathode, W_p is weight of the aluminum foil with cathode paste, W_0 is the weight of aluminum foil which used for electrode substrate, and R_s is the mass ratio of sulfur within the sulfur composite. The mass ratio of sulfur is according to results from thermogravimetric analysis.

4 Graphene-Sulfur Composite

4.1 Material Synthesis of Graphene Sulfur Composite

Graphene nanosheets used for sulfur composite synthesis was prepared from reduce reaction of graphene oxide. The graphene oxide was prepared from graphite powders (SP-1, Bay Carbon, MI, USA) using a modified Hummers method [117]. The preparation of graphene nanosheets I conducted was based on the following procedure: 70 mL concentrated hydro sulfuric acid was first poured into a round-bottom flask in an ice bath. 1 g graphite powder, 0.5 g sodium nitrate and 3 g KMnO4 were gradually added into hydro sulfuric acid in sequence. The mixture was stirred for 2 h and then diluted with distilled water. After then, 5% (wt%) hydrogen peroxide was gradually added into the solution. Once the color of the mixture changed to brilliant yellow, the reaction was completed and graphite oxide was generated. Then, the as-prepared graphite oxide was dispersed in distilled water and then exfoliated to generate graphene oxide nanosheets through sonication using an ultrasonic probe (Branson S-450D sonifier). After sonication, the brown suspension of graphene oxide nanosheets was poured into a round bottom flask and added with 10 ~ 20 μL hydrazine hydrate for further reduction [118]. The mixed solution was then refluxed at 100 °C for 2 hours to obtain graphene suspension. As the color of the solution gradually changed to dark black, the graphene suspension was received. Afterwards the suspension was centrifuged at 3000 rpm for 15

minutes to remove precipitate. The separated supernatant of the graphene suspension was vacuum dried at 80°C for 12 hours and powder-like dry graphene nanosheets were finally obtained.

The synthesis procedure of graphene/sulfur composite is as follows: 0.05 g graphene powder was mixed with 0.05 g sulfur powder by pestle and mortar. The mixture was then heated to 150 °C and maintained at that temperature for 3 hours under vacuum, during which the liquid sulfur was imbibed into the inner space between graphene nanosheets under capillary attraction.

4.2 Material Characterization of Graphene-Sulfur Composite

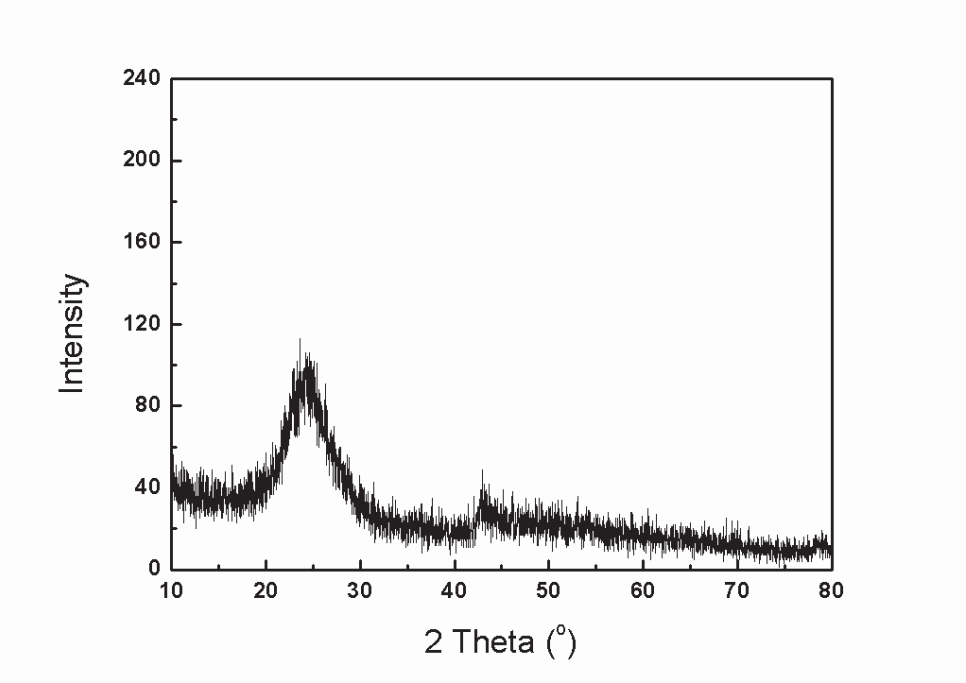

Figure 4.1 The XRD Patterns of Graphene-Sulfur Composite

The XRD pattern of graphene-sulfur composite is displayed in Figure 4.1, which only showed border diffraction peaks of graphene (carbon) between 20° and 30°. The disappearance of diffraction lines of crystalline sulfur has been reported in other sulfur composite synthesis [81, 114]. One possible reason for the vanishing of sulfur diffraction peaks in the composite is the phase transformation of sulfur during the synthesis process as the sulfur particles are imbedded between graphene monolayers.

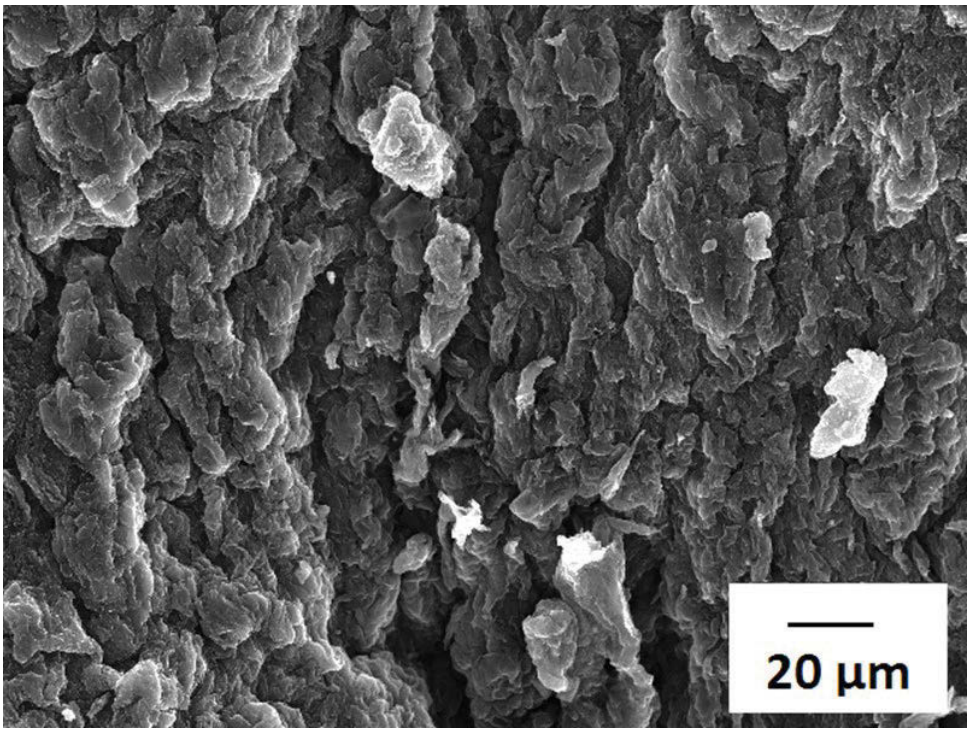

Figure 4.2 The Morphology of Graphene-Sulfur Composite

Figure 4.2 shows morphology of graphene-sulfur composite acquired from the scanning electron microscope without back-scattering, in which only the

morphology of corrugated graphene nanosheets can be observed. The energy dispersive X-ray elemental mapping was conducted to examine the element distribution within the composite.

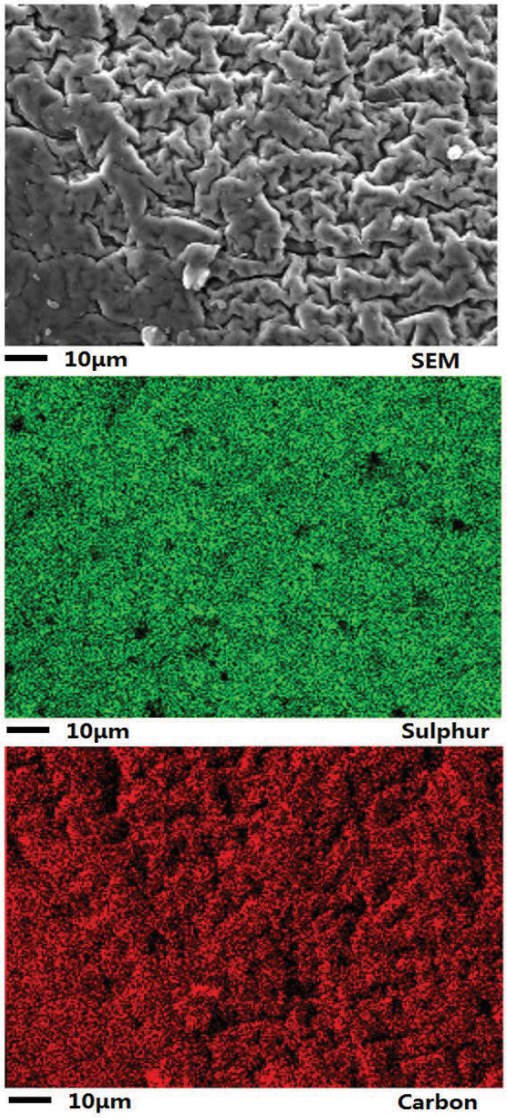

Figure 4.3 The EDS Element Mapping of Graphene-Sulfur Composite[2]

[2] This elemental mapping of graphene –sulfur composite was performed by Dr. David Wexler on JEOL 7001F field emission electron microscope (FESEM) at the University of Wollongong. The sample was first dispersed in solvent at sample preparation stage thus the morphology appears to be different from it in Fig 4.2.

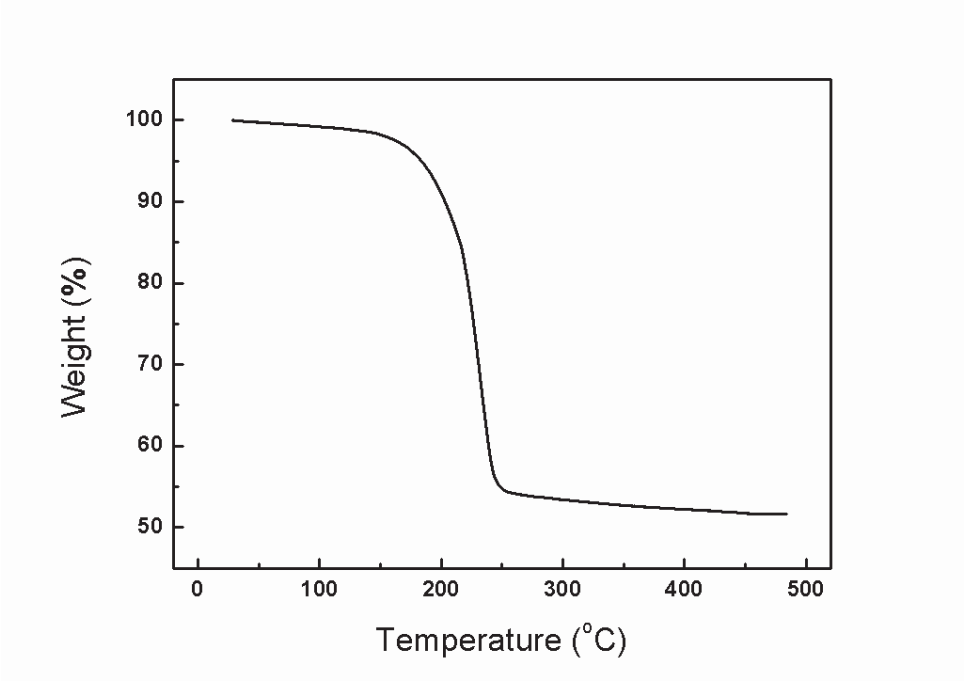

Figure 4.4 The Weight Loss Curve of Graphene-Sulfur Composite

The element mapping results showing in Figure 4.3 confirmed a uniform distribution of sulfur in graphene nanosheets at micro meter level. The homogeneous distribution of element sulfur within graphene nanosheets ensures the intimate electrical contacts between sulfur particles. Further thermal-gravimetric analysis verified the sulfur content in the synthesized graphene-sulfur composite was 48.4 % (wt%) (as shown in Figure 4.4).

4.3 Graphene-Sulfur Cathode Fabrication

A blend of synthesized graphene-sulfur composite material (80 wt%), carbon black (10 wt%), and polyvinylidene fluoride (10 wt%) was mixed with

N-methyl-2-pyrrolidone (NMP) to form a slurry. The slurry was then coated on aluminum foils with doctor-blade method. The coated aluminum foils were vacuum dried at 80 °C for 12 h. After the bake-out, the electrodes were pressed with molds to form a compact layer of active mass. Lithium foils were used as the negative electrode. Test batteries were assembled as type of CR2032 coin cells. The electrolyte used for battery tests was 1 mol/L lithium bis(trifluoromethane sulfone) imide (LiTFSI, $LiN(SO_2CF_3)_2$) salt in a mixed solvent of 1,2-dimethoxyethane (DME) and 1,3-dioxolane (DOX) (4:1 in volume ratio). The battery assembling was conducted in argon filled glove-box with both moisture and oxygen levels below 0.1 ppm.

4.4 Electrochemical Tests of Graphene-Sulfur Cathode

Figure 4.5 shows the cyclic voltammetry curve of a lithium battery with a graphene-sulfur cathode in its second sweep cycle, which provides more detailed information of equilibrium of electrochemical reaction within the full charge-discharge voltage range (1.0V-3.0V). Since graphene is electrochemically inert in the selected voltage range, the redox peaks can only be ascribed to the reactions between lithium ions and sulfur. The cathodic peak located at 2.4 V corresponds to the reduction of elemental sulfur to soluble polysulfides (Li_2S_x, $2<x<8$). The second cathodic peak at 2.1 V can be assigned to the further polysulfides to insoluble polysulfides (Li_2S or Li_2S_2). The sharp anodic peak around

2.4 V corresponds to the conversion of polysulfides to sulfur during the charge process. Thus the charge-discharge behavior of graphene-sulfur composite is in accordance with the typical sulfur cathodes [79].

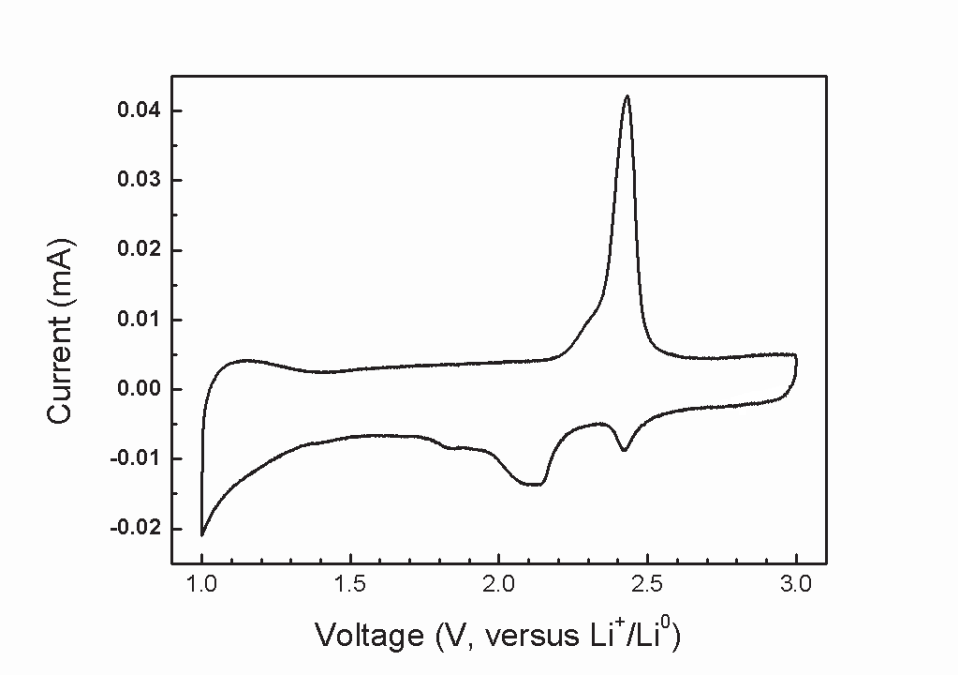

Figure 4.5 The Cyclic-Voltammetry Plot of Graphene-Sulfur Composite

Figure 4.6 shows the voltage-capacity curves of graphene-sulfur cathodes in their first discharge cycles at different current rates. Two discharge plateaus of sulfur can be distinguished in 0.1 C and 1.0 C discharge rates, which are consistent with the redox peaks in cyclic voltammetry plot. The voltage-capacity curves clearly showed the majority of discharge capacity of graphene-sulfur cathode is attributed to the second discharge plateau of sulfur (below 2.1 V). The voltage-capacity curves also revealed the change of discharge behavior of graphene-sulfur cathode under high

discharge rate. The voltage-capacity curves at 0.1 C and 1.0 C discharge rates present identical two-step reduction plateaus. However, the voltage-capacity curve at the current densities of 3344 mA/g (2.0 C) showed no voltage plateau but a fast declining slope, which indicates an incomplete reduction process of sulfur in graphene-sulfur cathode under fast discharge.

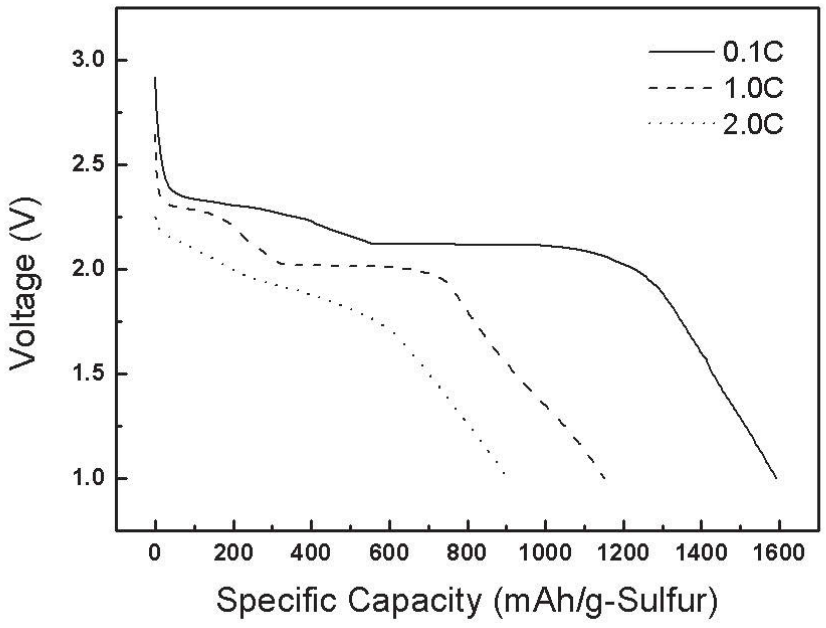

Figure 4.6 Voltage-Capacity Curves of Graphene-Sulfur Composite at Different Discharge Current Densities

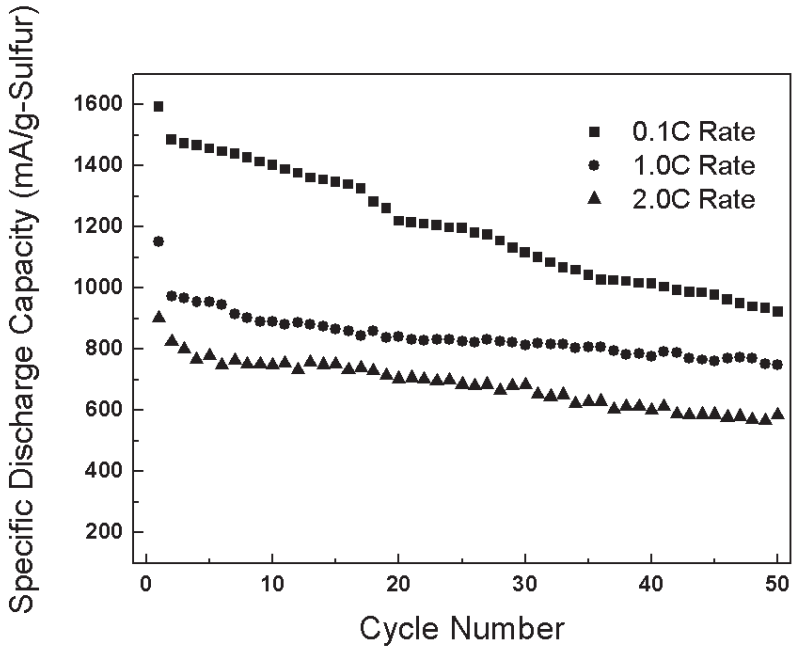

Figure 4.7 Specific Discharge Capacity of Graphene-Sulfur Composite at Different Current Densities

Figure 4.7 shows the specific discharge capacities of graphene-sulfur cathode under different current densities including 167 mA /g (0.1 C), 1672 mA /g (1.0 C) and 3344 mA /g (2.0 C). The graphene-sulfur cathode exhibits the highest specific discharge capacity of 1593 mAh /g-S in the initial cycle at 0.1C rate. The difference of specific discharge capacities achieved at varied current densities indicates a relatively good utilization of sulfur at low current rate. The graphene-sulfur cathode maintained high discharge capacity over 1400 mAh /g-S in the first 10 cycles and a specific discharge capacity of 923mAh /g-S in the 50th cycle under 0.1C discharge rate. The graphene-sulfur cathodes also exhibit the good performance on specific capacity at

higher current rate, the initial discharge capacities at 1.0 C and 2.0 C discharge rates are 1153 mAh /g and 902 mAh /g. The capacity retention rate of high discharge current appeared to be higher than that of low discharge current, the reason may be attributed to the low sulfur utilization rate at high current density and less insoluble polysulfides formation in the subsequent reactions.

The sulfur utilization rate has been significantly improved with synthesized graphene-sulfur composite cathode. With the deposit of sulfur within graphene nanosheets, the electrical insulating nature of sulfur has been modified by the highly conductivity of graphene nanosheets. The graphene-sulfur cathode has demonstrated dramatic improve of rate capability on sulfur cathode as it is capable of delivering full lithiation of sulfur content at 1.0 C rate. In addition, with the high mechanical strength and flexibility of graphene nanosheets, the graphene-sulfur cathode could accommodate the volume change of sulfur during the charge-discharge process and then improve the cycle stability of sulfur cathode during continuous charge-discharge process. Although the combination of graphene-sulfur as cathode offers a limited improvement on the cycle stability of Li-S battery, the problem of capacity fading over long cycles remains a challenge.

5 Carbon-Sulfur Composite (CS_2)

5.1 Material Synthesis of Carbon-Sulfur Composite

The solvent carbon disulfide was used for synthesis carbon-sulfur composite through a solution-based route. The carbon disulfide assisted sulfur/carbon composite synthesis procedure is as follows: 0.7 g sulfur was added in 15 ml carbon disulfide and immediately dissolved, and then 0.3 g finely ground Vulcan XC-72 carbon powder was added while the solution was mixed by a magnetic stirring at a medium speed. The solution was stirred and maintained at about 50 °C for 1 hour to allow evaporation carbon disulfide and precipitation of sulfur. The black precipitate was washed with ethanol and distilled water then vacuum dried.

5.2 Material Characterization of Carbon-Sulfur Composite

Figure 5.1 shows the XRD patterns of carbon-sulfur composite with carbon disulfide. Major diffraction peaks of sulfur matched well with the standard diffraction lines of sulfur (JCPDS card No. 08-0247), which can be indexed to the orthorhombic phase with the space group of Fddd. The diffraction peaks of carbon content are covered in the background and difficult to distinguish. The diffraction profile indicates no phase transformation of sulfur during the dissolution processing in carbon disulfide.

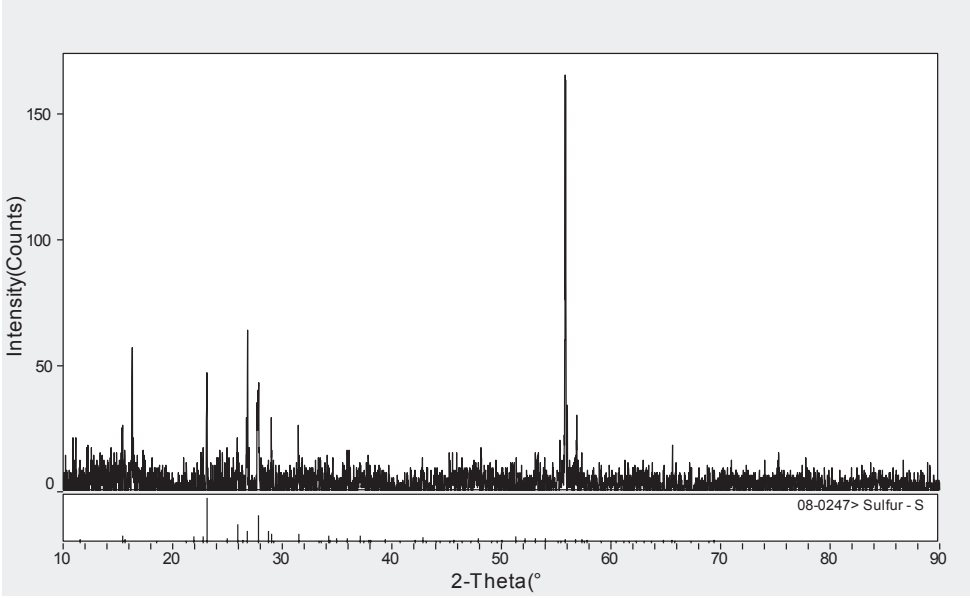

Figure 5.1 The XRD Patterns of Carbon-Sulfur Composite

Lower Peak plot is the Corresponding Standard Patterns of Sulfur

(JCPDS No 08-0247)

Figure 5.2 is the morphology of carbon-sulfur composite acquired with FESEM. The low magnification backscattered image (Figure 5.2a) of the as-prepared composite revealed the sulfur distribution within the material was not homogenous, some areas showed higher level of concentration of sulfur than others, and the size of bulk sulfur particles was about 3 - 15 μm, which is close to that of the ball-milling processed carbon-sulfur composite [53]. Therefore, the CS_2 solution processing has no significant effect in reducing the particle size of sulfur. The content of sulfur in the as-prepared material was determined by thermal-gravimetric analysis (TGA).

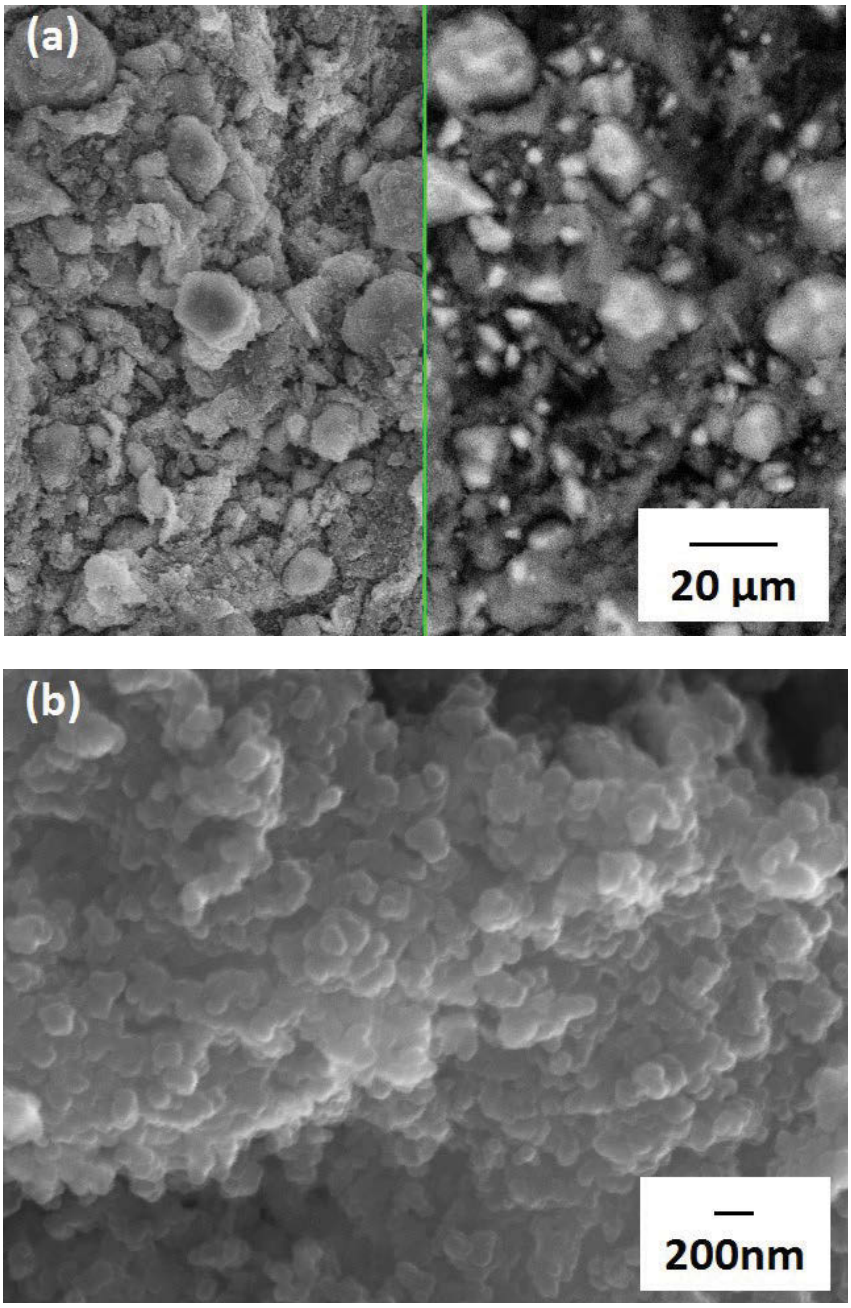

Figure 5.2 The Morphology of Carbon-Sulfur Composite

(a) Backscattered image, (b) SEM image.

The left part of (a) is the ordinary SEM image, and the right part of (a) is the corresponding back-scatter image. Those highlight areas in back-scattered image represents element Sulfur.

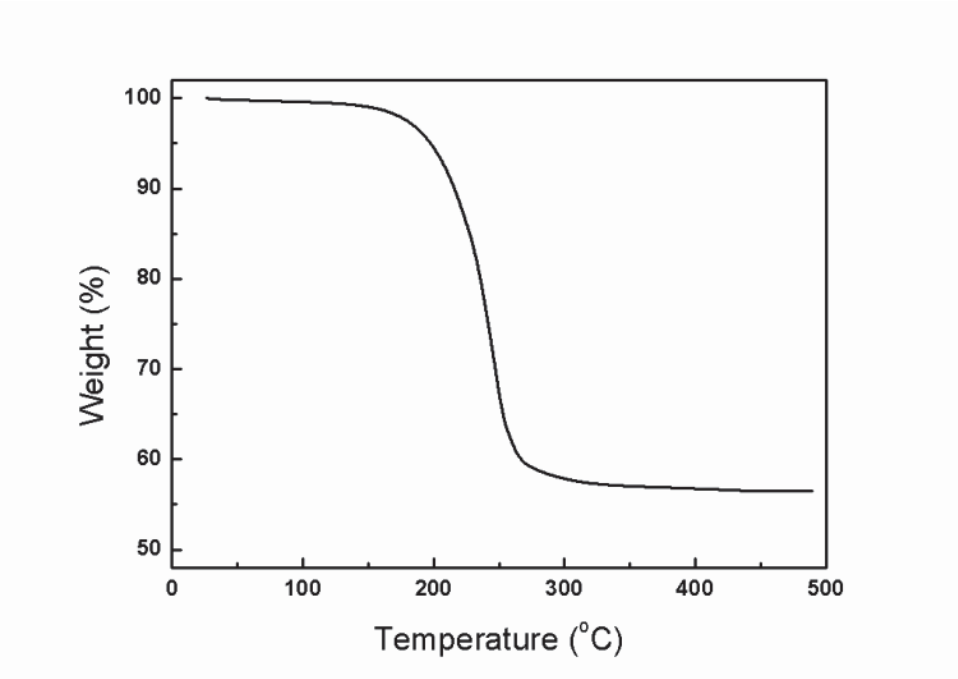

Figure 5.3 The Weight Loss Curve of Carbon-Sulfur Composite in Thermal-Gravimetric Analysis

Figure 5.3 shows the TGA weight loss curve of the as-prepared carbon-sulfur composites. The synthesized material contains 43.55 % (wt%) sulfur, which is lower than the nominal value (50%). The decreased sulfur mass ratio after synthesis may be attributed to the measures to remove the residual carbon disulfide, during which recrystallized sulfur was washed off from the surface by ethanol and distilled water.

5.3 Carbon-Sulfur Cathode Fabrication

A blend of synthesized sulfur composite material (80 wt%), carbon black (10 wt%), and PVDF (10 wt%) was mixed with NMP to form a slurry. The slurry was then coated on aluminum foils with roll-pressing method. The coated aluminum foils

were vacuum dried at 80 °C for 12 h. After the bake-out, the electrodes were cut into round shape with a diameter of 14 mm and pressed with molds to form a compact layer of active mass. Lithium foils were used as the negative electrode. Test batteries were assembled as type of CR2032 coin cells. The electrolyte used for battery tests was 1 mol/L LiTFSI salt in a mixed solvent of DME/DOX (4:1 in volume ratio). The battery assembling was conducted in argon filled glove-box with both moisture and oxygen levels below 0.1 ppm.

5.4 Electrochemical Tests of Carbon-Sulfur Cathode

Figure 5.4 shows the cyclic voltammetry curves (1^{st} cycle and 2^{nd} cycle) of the as-prepared carbon-sulfur cathode in the voltage range between 1.0V and 3.0 V. Two cathodic peaks in the first sweep cycle indicate the two-stage reduction processes of sulfur in the cathode. The first and the second cathodic peak at around 2.25 V and 1.9 V correspond to the reduction of elemental sulfur to high order polysulfides and low order polysulfides, respectively. The overlapped anodic peaks in the first sweep cycle at 2.5 V and 2.6 V represent a reversible process from polysulfides to elemental sulfur. In the second sweep cycle, the two reduction peaks shifted to 2.3 V and 2.0 V and the gap between two peaks became more obvious. The anodic peak at 2.6 V disappeared and left a single anodic peak narrowed to 2.5V. The shifts of peak voltages are attributed to the increased electrochemical activity (reversibility) and sulfur utilization rate of sulfur cathode.

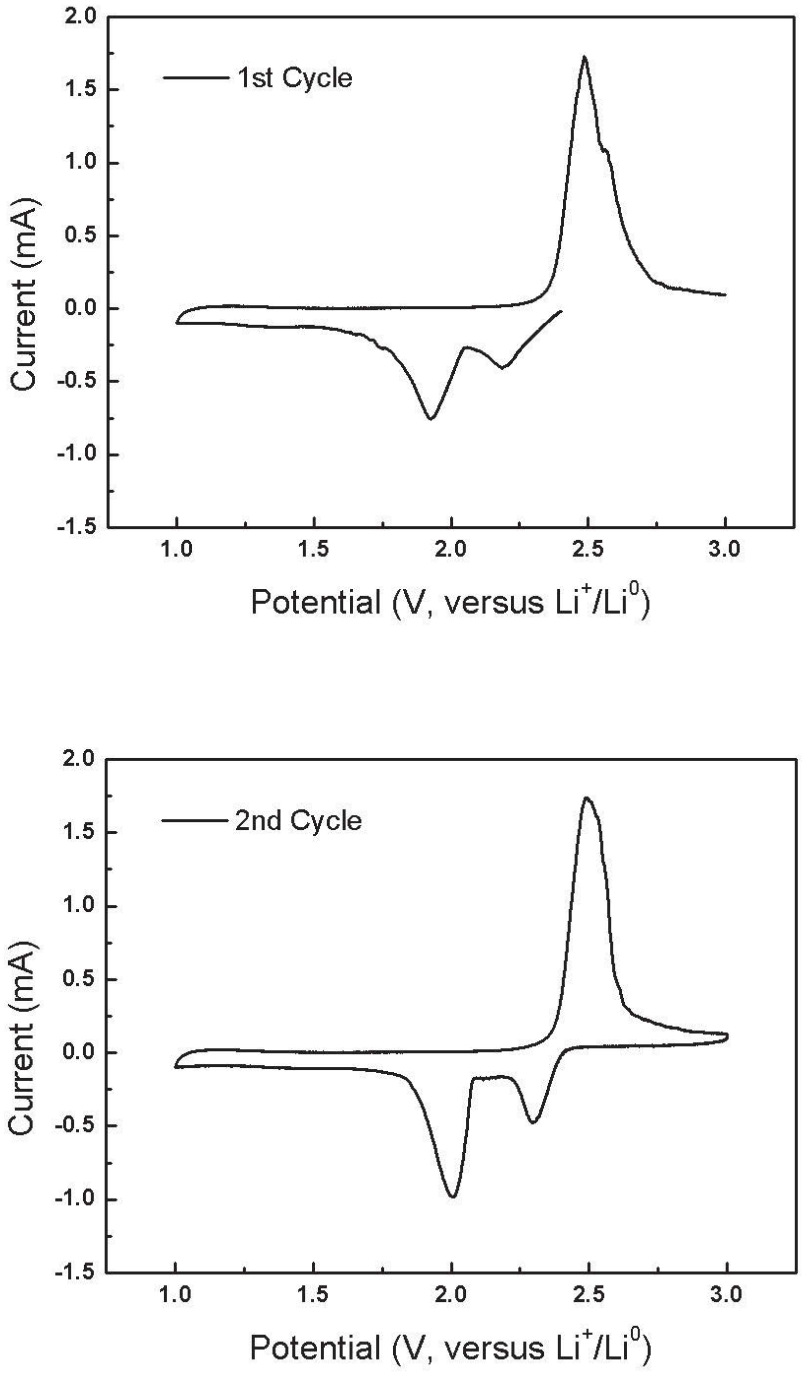

Figure 5.4 The Cyclic-Voltammetry Plots of Carbon-Sulfur Composite

Figure 5.5 shows the voltage-capacity curves of carbon-sulfur cathodes. It can be conclude that sulfur utilization rate of cathode at the initial cycle decreases with the increase of the current density, comparing with discharge voltage curves at 0.1C and 0.2C rate, the second discharge plateau was shortened 0.4 C rate, which leads to a decreased capacity. The low coulombic efficiency is also a major defect of the as-prepared cathode material.

The charge-discharge cycle tests at current densities higher than 0.5 C all exhibited short cycle life time along with large shaking in voltage-capacity curves which could not be used for analysis. This is attributed to the limited conductivity and structural stability of amorphous carbon in the composite.

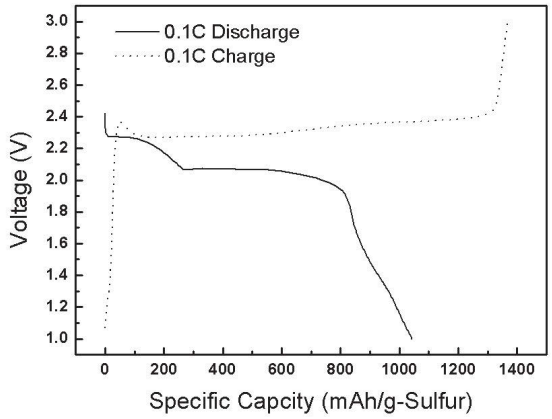

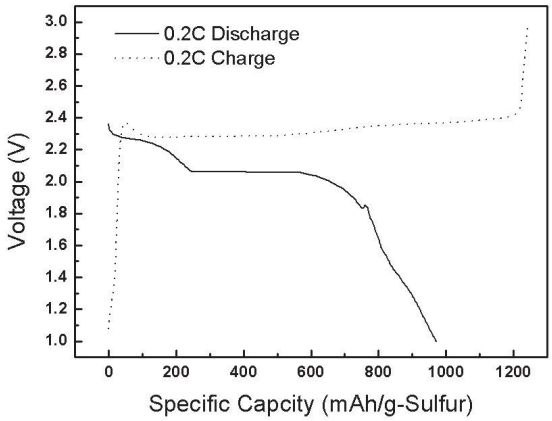

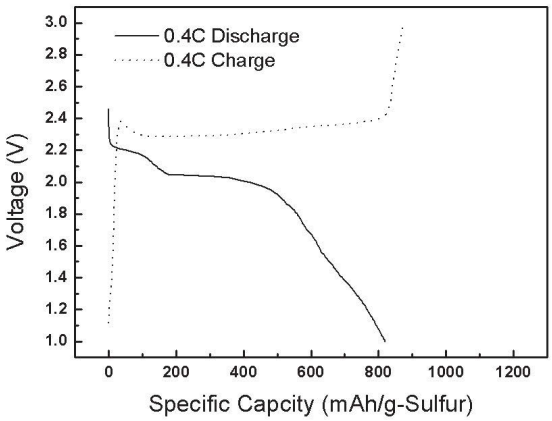

Figure 5.5 Voltage-Capacity Curves of Carbon-Sulfur Composite at Different Discharge Current Densities

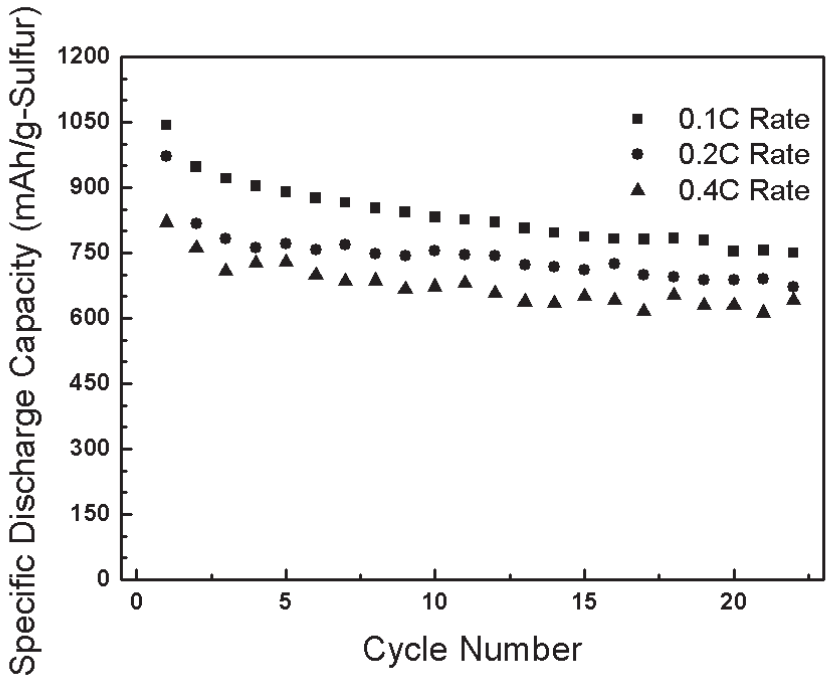

Figure 5.6 Specific Discharge Capacities of Carbon-Sulfur Composite at Different Current Densities

Figure 5.6 shows the specific discharge capacity of as-prepared carbon-sulfur cathodes at different current densities of 167 mAh/g (0.1 C), 334 mAh/g (0.2 C) and 669 mAh/g (0.4 C), respectively. The initial specific discharge capacity of as-prepared sulfur cathode is 1043 mAh/g at 0.1C, 971 mAh/g at 0.2 C, and 820 mAh/g at 0.4C. According to those cycling data, the capacity fading phenomenon of the as-prepared cathode material is also obvious, the capacity retention rate at 0.1 C discharge rate after 20 charge-discharge cycles was less than 80%.

6 Carbon-Sulfur Composite (DMSO)

6.1 Material Synthesis of Carbon-Sulfur Nanocomposite

The synthesis of carbon-sulfur nanocomposite through sonication is according to the following procedure. In the first step, 0.7g sulfur powder was dissolved in 50 ml DMSO through sonication by a high energy ultrasonic probe (Branson S-450D sonifier). Then, 0.3g finely ground Vulcan XC-72 carbon powder was added and dispersed into the solution. The solution was kept under sonication for another 5 minutes. The solution was then stirred and cooled at room temperature, during which sulfur and carbon particles formed sulfur/carbon composite. After that, the black precipitate was washed with ethanol and distilled water several times to eliminate DMSO residual, then dried under vacuum at 100°C for 8 hours to evaporate moisture.

6.2 Material Characterization of Carbon-Sulfur Nanocomposite

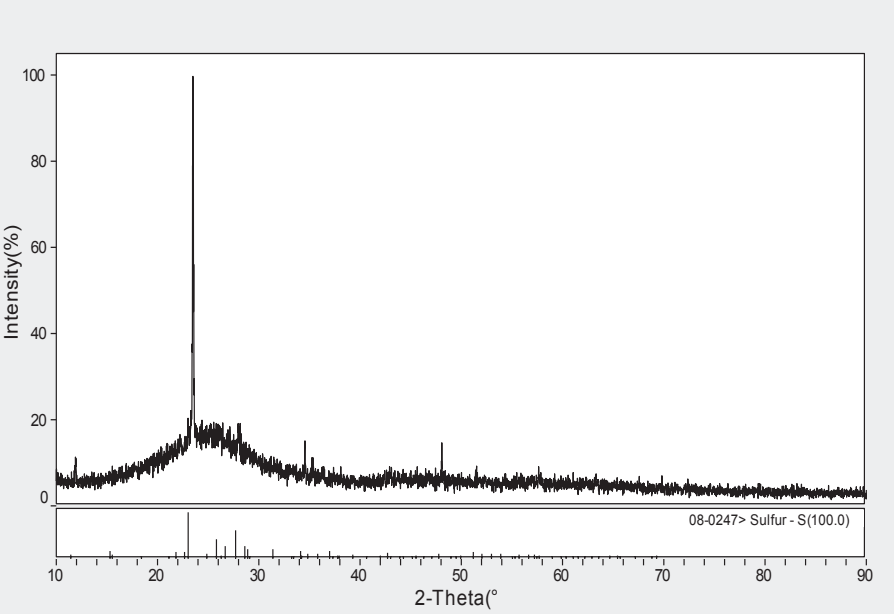

Figure 6.1 The XRD Patterns of Carbon-Sulfur Nanocomposite

Lower Peak plot is the Corresponding Standard Patterns of Sulfur

(JCPDS No 08-0247)

Figure 6.1 shows the XRD patterns of the pristine sulfur powders and the as-prepared carbon-sulfur nanocomposites, respectively. All diffraction peaks of sulfur match very well with the standard diffraction lines of sulfur (JCPDS card No. 08-0247), which can be indexed to the orthorhombic phase with the space group of Fddd. The XRD pattern of carbon-sulfur nanocomposites consists of diffraction peaks of sulfur and a broad diffraction peak at 25◦, which corresponds to amorphous carbon in the composite. This indicates that sulfur re-crystallized after the solution-based processing by DMSO.

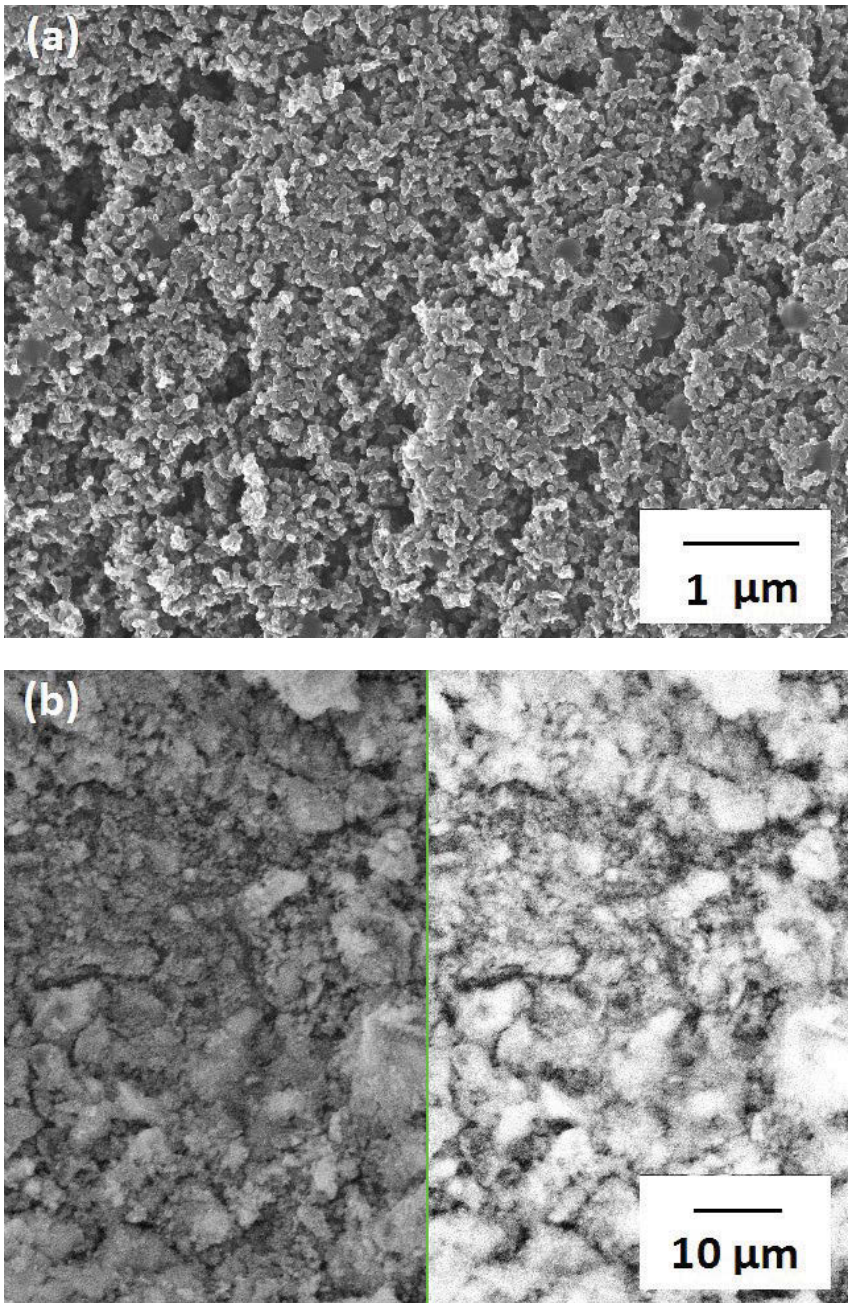

Figure 6.2 The Morphology of Carbon-Sulfur Composite

(a) SEM image (b) backscattered image

The left part of (b) is the ordinary SEM image, and the right part of (b) is the corresponding back-scatter image. Those highlight areas in back-scattered image represents element Sulfur.

The morphology and distribution of sulfur of the as-prepared carbon-sulfur nanocomposite was analyzed by FESEM with back-scatter imaging. A SEM image of carbon-sulfur nanocomposite is shown in Figure 6.2 (a), from which the mixture of super-fine nanocomposite particles can be clearly identified. During the dissolution processing, sulfur was dissolved by the solvent DMSO and intimately mixed with carbon matrix. During the cooling process, the re-crystallized spherical sulfur particles were intimately imbedded into the carbon matrix and formed a homogeneous dispersion of sulfur within the composite. The crystal size of sulfur has been significantly reduced to a range of a few tens to a hundred nanometers after this dissolution and re-crystallization process. Figure 6.2 (b) shows the back-scattered electron image of carbon-sulfur nanocomposite at a low magnification, from which the uniform distribution of sulfur in carbon matrix can be seen. The highlight area represents sulfur element, which is mixed well with carbon. Therefore, the solution-based processing can allow the formation of carbon-sulfur nanocomposite containing crystalline sulfur with a significantly reduced particle size of sulfur.

The content of sulfur in carbon-sulfur nano composite was determined by thermal gravimetric analysis. Figure 6.3 shows the weight loss curve of the as-prepared carbon-sulfur nanocomposite. The nanocomposite contains 64.74 % (wt%) sulfur, which is slightly lower than the nominal value (70 wt%). The difference between the

actual sulfur mass ratio and theoretical value is due to a small amount of sulfur remaining dissolved in DMSO solvent after the synthesis process.

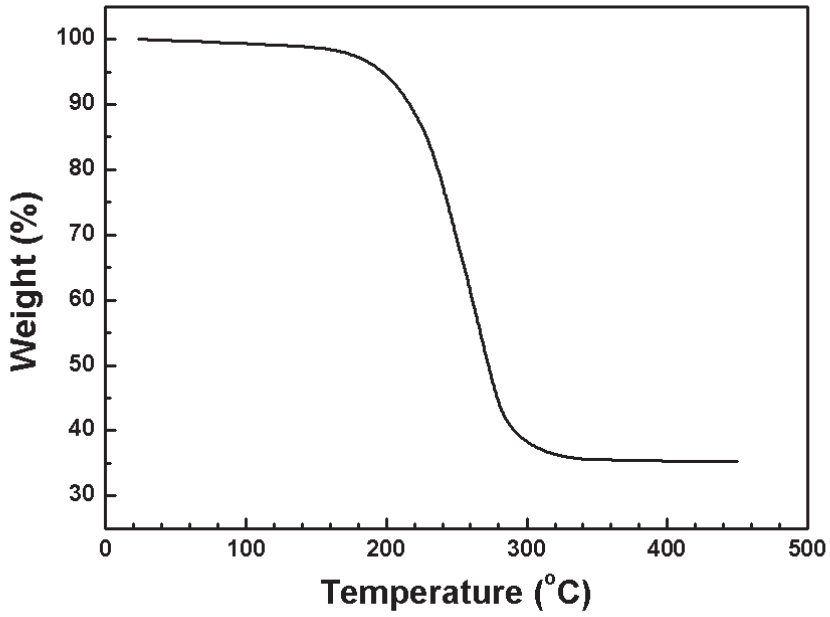

Figure 6.3 The Weight Loss Curve of Carbon-Sulfur Nano Composite in Thermal-Gravimetric Analysis

6.3 Carbon-Sulfur Cathode Fabrication

A blend of synthesized sulfur composite material (80 wt%), carbon black (10 wt%), and PVDF (10 wt%) was mixed with NMP to form a slurry. The slurry was then coated on aluminum foils roll-pressing method. The coated aluminum foils were vacuum dried at 80 °C for 12 h. After the bake-out, the electrodes were cut into round shape with a diameter of 14 mm and pressed with molds to form a compact layer of active mass. Lithium foils were used as the negative electrode. Lithium foils

were used as the negative electrode. Test batteries were assembled as type of CR2032 coin cells. The electrolyte used for battery tests was 1 mol/L LiTFSI salt in a mixed solvent of DME/DOX (4:1 in volume ratio). The battery assembling was conducted in argon filled glove-box with both moisture and oxygen levels below 0.1 ppm. The reference sulfur cathodes were also prepared for the electrochemical tests, the components of reference sulfur cathode include sulfur (80 wt%), carbon black (10 wt%), and PVDF (10 wt%).

6.4 Electrochemical Tests of Carbon-Sulfur Cathode

Figure 6.4 shows the cyclic voltammetry (CV) curves of the carbon-sulfur nanocomposite electrode in the voltage window at 1.0 V to 3.0 V. As carbon is electrochemically inert in this voltage range, the redox peaks can only be ascribed to the redox reactions associated with sulfur and lithium ions. In the first cycle, two cathodic peaks are identified, which can be assigned to the reduction processes of sulfur. The first cathodic peak at around 2.2 V corresponds to the reduction of elemental sulfur to polysulfides. The second cathodic peak at about 1.94 V corresponds to further reduction of polysulfides and formation of Li_2S_2 and Li_2S. The anodic peak at 2.5 V represents the conversion process from polysulfides to elemental sulfur. From the second cycle, the reduction peaks and the oxidation peak shifted slightly to a higher potential. The shifts of peak voltages are associated with

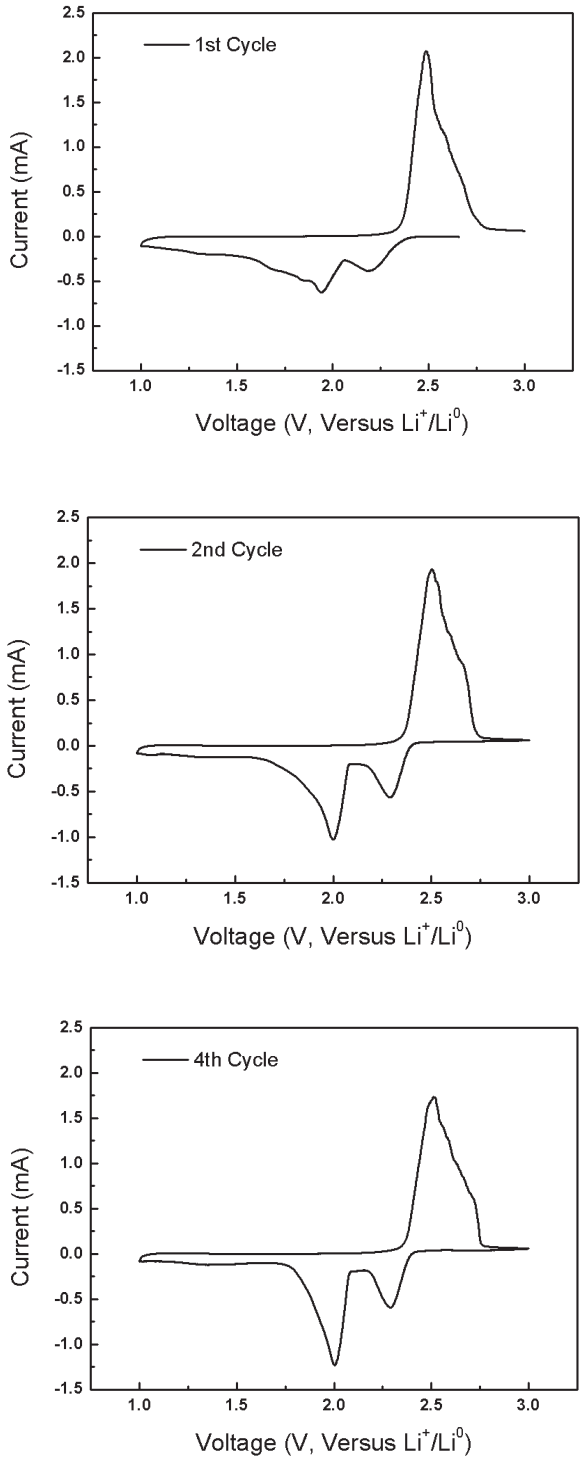

Figure 6.4 The Cyclic-Voltammetry Plots of Carbon-Sulfur Nanocomposite

gradually improved reversibility of electrochemical reactions, implying enhanced sulfur utilization in the electrodes.

Figure 6.5 displays the charge-discharge profiles of carbon-sulfur nanocomposite electrodes at different current densities. Two discharge plateaus can be distinguished in the voltage ranges of 2.4 V – 2.1 V and 2.1 V – 1.5 V under different current densities. The first discharge plateau is relatively shorter, while the second discharge plateau extends longer and contributes to the majority of the discharge capacity. These discharge plateaus are in accordance with two cathodic peaks showed in the cyclic voltammetry curves. The second discharge stages present a long horizontal plateau, which implies a complete reduction process from sulfur to polysulfides. The voltage-capacity curves also revealed the low coulombic efficiency of as-prepared sulfur cathodes as the charge capacities are much higher than the discharge capacities under varied charge-discharge rates.

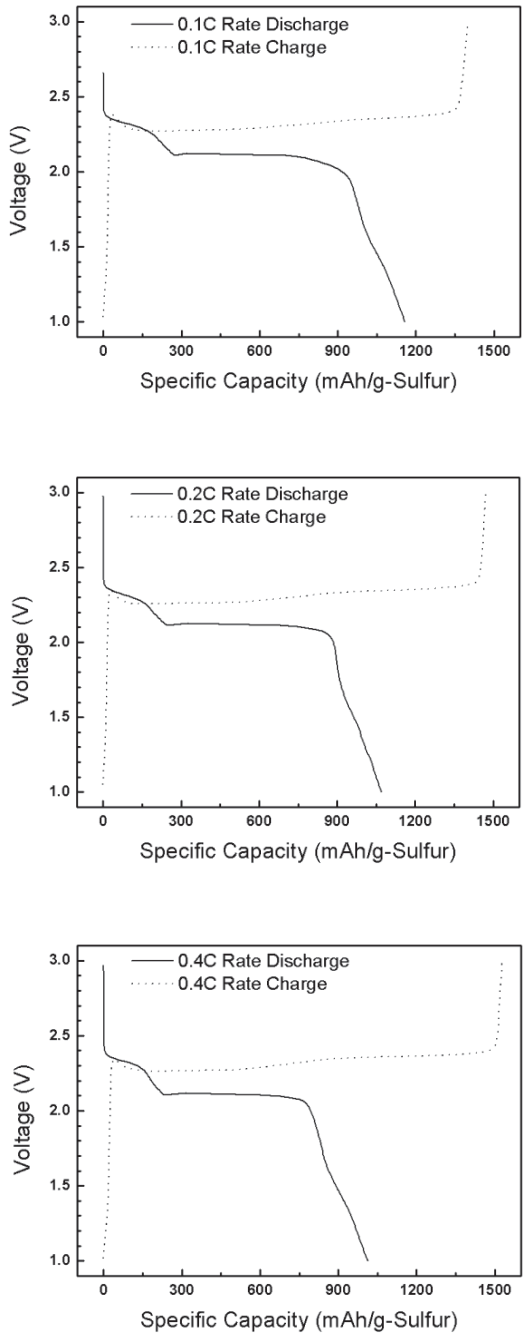

Figure 6.5 Voltage-Capacity Curves of Carbon-Sulfur Nanocomposite at Different Current Densities

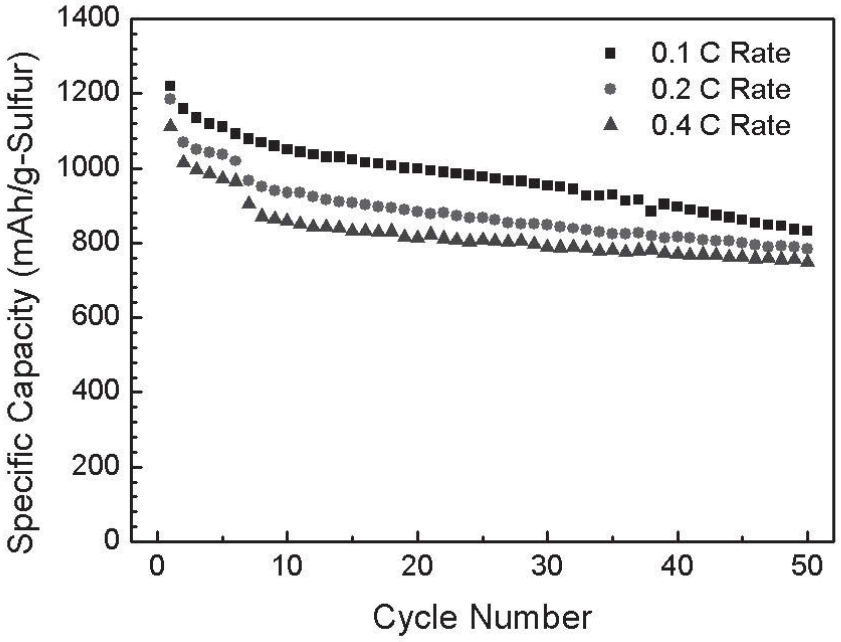

Figure 6.6 Specific Discharge Capacity of Carbon-Sulfur Nanocomposite at Different Current Densities

Figure 6.6 shows the cycle performance of carbon-sulfur nanocomposite electrodes at current densities of 167 mAh/g (0.1 C), 334 mAh/g (0.2 C) and 669 mAh/g (0.4 C), respectively. The as-prepared sulfur cathodes delivered the highest specific discharge capacity of 1220 mAh/g at 0.1 C in the first cycle. The cathode has a slightly declined capacity with cycle number increasing, and managed to maintain a specific capacity of 832 mAh/g at the 50th cycle. The carbon-sulfur nanocomposite electrodes also achieved the highest discharge capacities of 1184 mAh/g at 0.2 C and 1111 mAh/g at 0.4 C, and the capacity retention of 784 mAh/g (0.2C) and 749 mAh/g (0.4C) after 50 cycles, respectively. This demonstrates an enhanced cycle

stability of the as-prepared nano composites at current rates below 0.4 C. However, the continuous capacity fading (more than 20% within 50 cycles) revealed the challenge of maintaining cycle stability of as-prepared sulfur cathodes. The solution-based synthesis process can help achieve a well dispersion of nano-sized sulfur within a carbonaceous composite, but the electrochemical stability of sulfur cathode is also depend on other components in electrodes and electrolyte system [61, 119]. The carbon material used in material synthesis is the drawback for the electrochemical performance of as-prepared sulfur composite, the relatively low conductivity of amorphous carbon (compared with graphene) can only allow cathode material achieves stable charge/discharge cycle at relatively low current rates. The solution process can obtain a reduced particle size of sulfur and well-distributed sulfur in carbon matrix, but cannot strongly hold sulfur on carbon matrix. The volume change of sulfur during cycling could degrade the connections between carbon and sulfur, inducing the gradual decrease of capacity.

Figure 6.7 displays the electrochemical impedance spectroscopy (EIS) of the carbon-sulfur nanocomposite electrode and the pristine sulfur electrode, respectively. In the high frequency region, the impedance response displays a semicircle loop and the corresponding diameter represents the charge transfer resistance at the electrode/electrolyte interface. From the impedance plot, it is evident that the carbon-sulfur nanocomposite electrode demonstrates a much

lower charge transfer resistance than that of the pristine sulfur electrode. This effect confirms that the nanocomposite architecture significantly increased the charge transfer process in the electrode, and therefore, improved the electrochemical performance of the lithium-sulfur batteries.

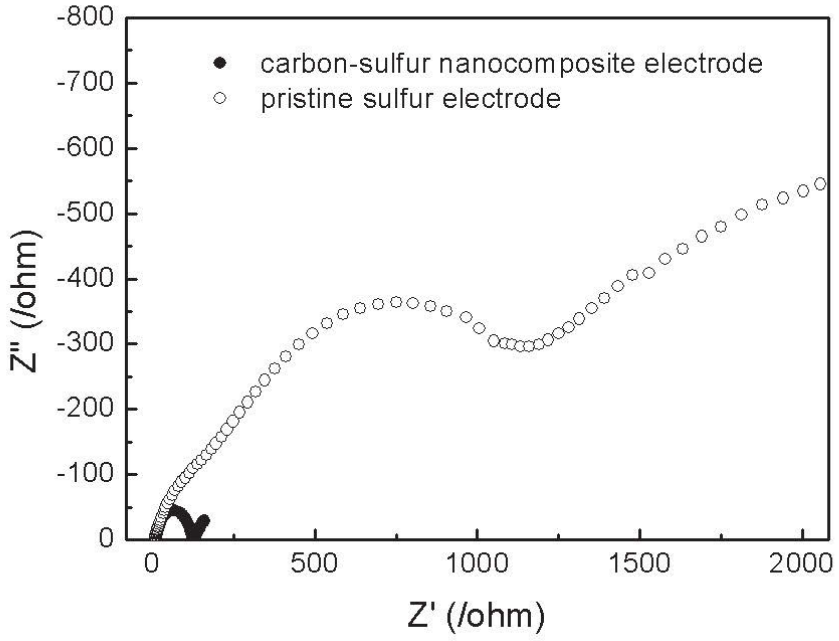

Figure 6.7 Electrochemical Impedance Plot of sulfur-carbon nanocomposite and reference sulfur cathode

7 Mesoporous Carbon-Sulfur Composite

7.1 Material Synthesis of Mesoporous Carbon-Sulfur Composite

Based on the established procedure [120], mesoporous carbon materials were synthesized from mesoporous silica template. The synthesis process of template includes the following steps: 1 g Pluronic P123 ($PEO_{20}PPO_{70}PEO_{20}$) was dissolved in 30 ml of hydrochloric acid (2 mol /L) at 38 °C. 2 g Tetraethyl orthosilicate was then added into the above solution and stirred for 5 minutes. The solution was kept still for at least 24 hours before transferred into autoclave. After the mixture was heated in the autoclave for 24 hours at 100 °C, the precipitation was filtered, dried and then heated in tube furnace filled with air atmosphere at 550 °C. Thus the preparation of silica template was completed. To synthesize mesoporous carbon from the as-prepared template, 0.5 g sucrose was first dissolved in 2.5 ml hydro sulfuric acid (0.3 mol/L), and then 0.5 g silica particles was dispersed in the solution. After 1 hour sonication, the mixture was heated at 100 °C for 6 h, then at 160 °C for another 6 h. The precipitate was heated in nitrogen atmosphere at 900 °C. The carbonized composite was soaked in hydrofluoric acid (2.5 mol /L) for 8 hours to remove residual of silica. Remained mesoporous carbon was washed and vacuum dried for further characterization.

I have conducted both melt-diffusion technique and solution-sonication technique

to synthesize sulfur/mesoporous carbon composites. The solution-sonication synthesis of sulfur/mesoporous carbon composites is according to the same procedure as that for carbon–sulfur nanocomposite. At first, 0.25 g sulfur powder was dissolved in 50 ml DMSO through sonication by a high energy ultrasonic probe (Branson S-450D sonifier). Next, 0.05g mesoporous carbon powder was added and dispersed into the solution. The solution was kept under sonication for another 5 minutes and then cooled while stirred at room temperature. After that, the black precipitate was washed with ethanol and distilled water several times to eliminate DMSO residual, then dried under vacuum at 100°C for 8 hours.

The melt-diffusion technique was also employed to synthesis sulfur/mesoporous carbon composite as a reference sample. The thermal synthesis procedure of mesoporous carbon/sulfur composite is as follows: 0.05 g mesoporous carbon powder was mixed with 0.05 g sulfur powder and fine ground. The mixture was then heated to 150 °C and maintained at that temperature for 3 hour under vacuum, during which the liquid state sulfur flow into interchannels of mesoporous carbon and imbibed in the inner space under capillary attraction.

7.2 Material Characterization of Mesoporous Carbon-Sulfur Composite

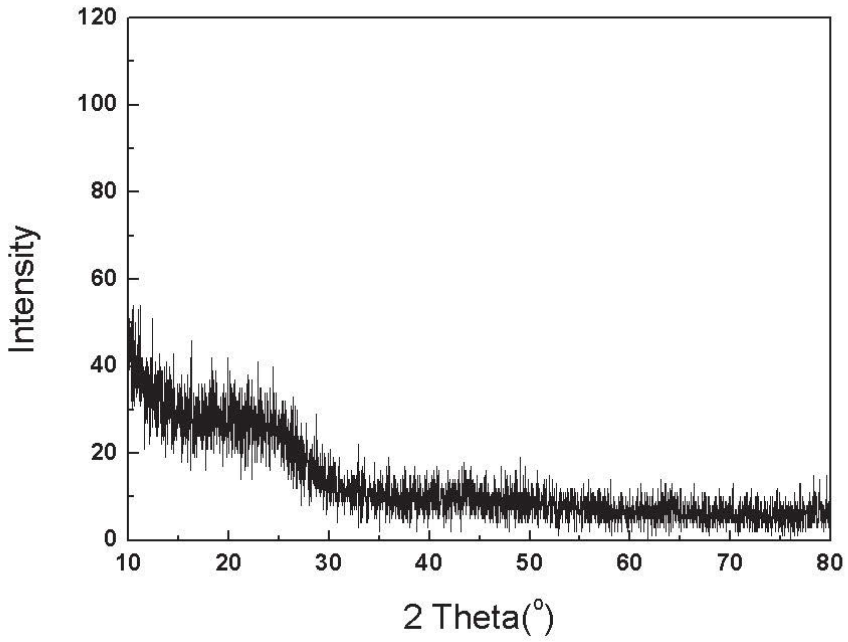

Figure 7.1 The XRD Patterns of Solution-Synthesized Mesoporous Carbon-Sulfur Composite

The XRD pattern of mesoporous carbon-sulfur composite (type I, synthesized through solution-based process) is displayed in Figure 7.1. The XRD profile of solution-based synthesized mesoporous carbon-sulfur composite only showed border diffraction peaks of carbon from 15° to 30°. The diffraction pattern of crystalline sulfur disappeared after the synthesis process.

Figure 7.2 shows morphology of thermal-synthesized mesoporous carbon-sulfur composite acquired from the scanning electron microscope. The SEM image clearly

showed the morphology of sulfur filled mesoporous carbon.

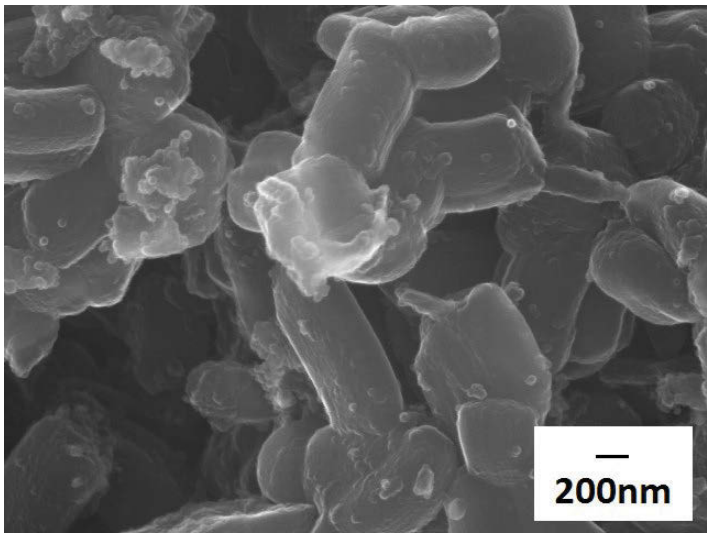

Figure 7.2 The Morphology of Thermal-Synthesized Mesoporous Carbon-Sulfur Composite

7.3 Mesoporous Carbon-Sulfur Cathode Fabrication

A blend of synthesized mesoporous carbon-sulfur composite material (80 wt%), carbon black (10 wt%), and PVDF (10 wt%) was mixed with NMP to form a slurry. The slurry was then coated on aluminum foils doctor-blade method. The coated aluminum foils were vacuum dried at 80 °C for 12 h. After the bake-out, the electrodes were pressed with molds to form a compact layer of active mass. Lithium foils were used as the negative electrode. Test batteries were assembled as type of CR2032 coin cells. The electrolyte used for battery tests was 1 mol/L LiTFSI salt in a

mixed solvent of DME/DOX (4:1 in volume ratio). The battery assembling was conducted in argon filled glove-box with both moisture and oxygen levels below 0.1 ppm.

7.4 Electrochemical Tests of Mesoporous Carbon-Sulfur Cathode

Figure 7.3 displays the discharge profile of solution synthesized mesoporous carbon sulfur composite. The as-prepared mesoporous carbon-sulfur composite showed negligible capacity and no discharge patterns as sulfur cathode in voltage range from 1.0 V to 3.0 V, which corresponds with the XRD result (see Figure 7.1).

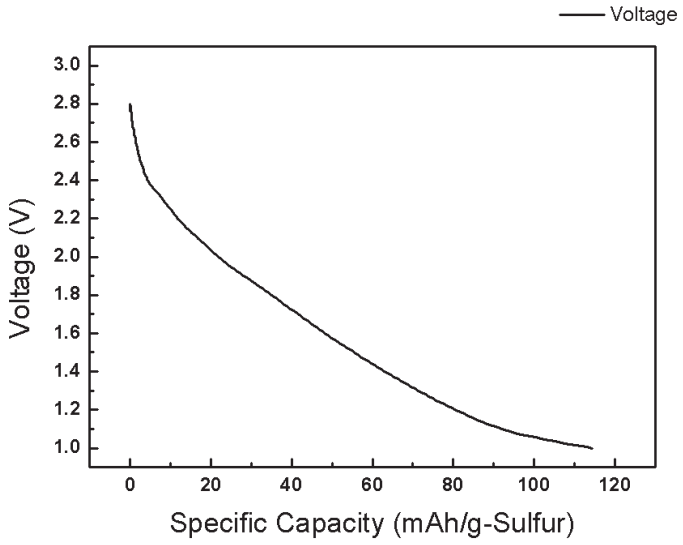

Figure 7.3 Voltage-Capacity Curves of Solution-Synthesized Mesoporous Carbon-Sulfur Cathode

The results from electrochemical tests of solution synthesized material revealed ineffectiveness of solution-sonication synthesis of sulfur composite with

mesoporous carbon. There are a few reasons that may cause the failure of the experiment. Firstly, the mesoporous carbon used for the material synthesis has the average pore size below 50 nm, which is much smaller than the particles size of sulfur after the sonication treatment in DMSO solvent (about 200nm). Thus the sulfur particles can hardly be transferred into the inner channels during the synthesis process. Secondly, the solution-sonication synthesis method has its own limitation on experiment parameters such as temperature, and reaction time. In a typical melt-diffusion synthesis of porous carbon/sulfur composite, the mixture of precursor is usually maintained to a temperature above 150° C for 4 hours to give sufficient time for the liquid state sulfur to flow into carbon matrix [81]. Thermal treatment with a temperature of 750 ° C and long process time was also used to form evaporated sulfur to cover the surface of porous carbon [92]. The high temperature and long synthesis time is difficult to achieve with the solution-sonication synthesis method due to the limitation such as control parameters of equipment, properties of solvents, etc. Since the sulfur particles can neither be transferred into the inner channels nor be dispersed on the outside of the mesoporous carbon rods, the amount of sulfur attached on mesoporous carbon after the synthesis is negligible. The above hypothesis was validated by the cycle test on the thermal synthesized mesoporous carbon-sulfur composite.

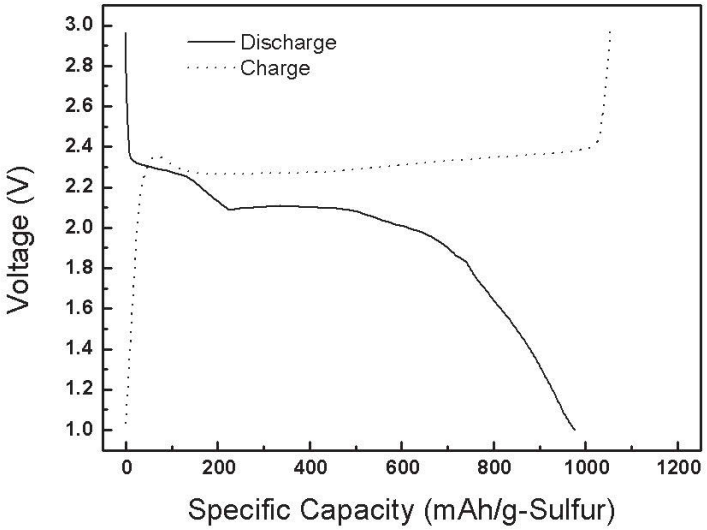

Figure 7.4 Voltage-Capacity Curves of Thermal-Synthesized Mesoporous Carbon-Sulfur Composite

Figure 7.4 is the voltage-capacity curve of mesoporous carbon-sulfur cathode prepared through melt-diffusion synthesis process. The discharge curve clearly showed the two-step sulfur reduction reaction in a discharge process with the high coulombic efficiency of a complete charge-discharge cycle, which indicates the highly reversible sulfur redox reactions in conjunction with the high conductivity networks within mesoporous carbon. In comparison with previously prepared carbon-sulfur composites (as described in Chapter 5 and Chapter 6), the mesoporous carbon-sulfur material from melt-diffusion synthesis process exhibits higher coulombic efficiency as cathode material.

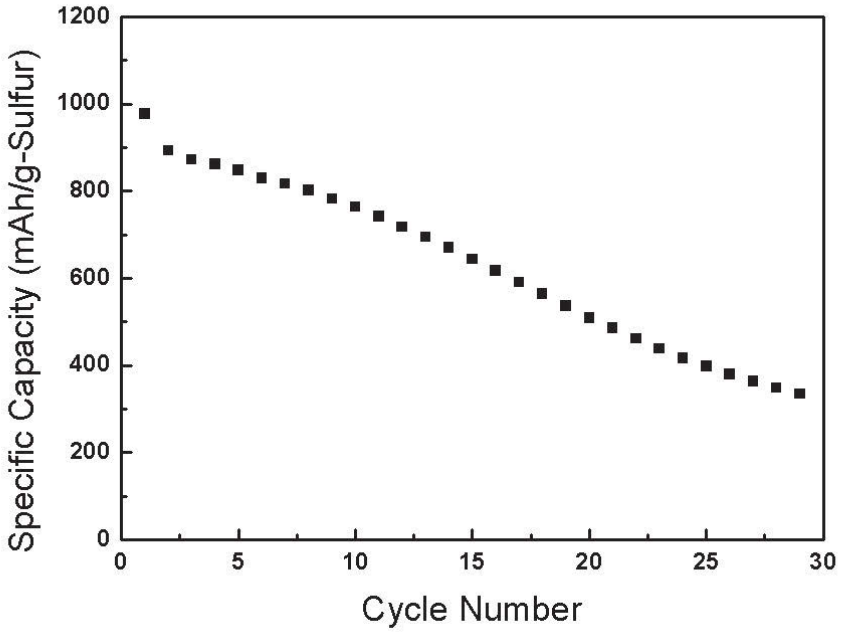

Figure 7.5 Specific Discharge Capacity of Thermal-Synthesized Mesoporous Carbon-Sulfur Nanocomposite

Figure 7.5 shows the cycle performance of thermal-synthesized mesoporous carbon-sulfur nanocomposite electrodes at current density of 100 mAh/g [3]. The as-prepared sulfur cathodes delivered a theoretical specific discharge capacity of 977 mAh/g in the first cycle. However, the cathode showed serious capacity fading with the first 30 cycles. After 30 cycles discharge, the theoretical specific discharge capacity of the cathode was 311 mAh/g. The continuous capacity loss of as-prepared cathode reveals that the modifications of synthesis techniques are necessary for sulfur-mesoporous carbon composites.

[3] The current density was calculated based on the theoretical value of sulfur content in the composite. The TGA data for the mesoporous carbon-sulfur composite was unavailable due to the TG analyzer malfunction.

8 Conclusions

In order to investigate the correlation between morphology of carbon material and the performance of composite sulfur cathode, graphene-sulfur composite was synthesized with the one-step melt-diffusion process and tested as cathode material. The as-prepared graphene-sulfur cathode exhibits the highest specific capacity of 1593 mAh/g at 0.1C discharge rate, which is equivalent to 95% sulfur utilization rate. The graphene-sulfur cathodes also achieved high capacities of 1153 mAh /g-S at 1.0 C, and 902 mAh /g-S at 2.0 C discharge rate. The continuous charge-discharge cycles under high current densities revealed the great improvement of graphene-sulfur cathode on rate capability. The composite material fully utilized the high electrical conductivity, high surface area and mechanical flexibility of graphene. With the homogenous distribution of sulfur within graphene nanosheets, the problem of sulfur's insulating nature can be effectively overcome. Although the as-prepared graphene-sulfur cathode has degrades on long-term cycling, graphene based sulfur composites are still one of those promising candidates as cathode materials for Li-S battery.

A solution-based synthesis technique has been developed to investigate the factor of sulfur particle size on the performance of sulfur cathode. With the joint force of sonication and dissolution-crystallization process, this method can significantly reduce the particle size of sulfur to hundreds of nano meters in the final product.

The synthesized carbon-sulfur composite have both small size and homogeneous size dissolution of sulfur within the amorphous carbon matrix. The as-prepared sulfur cathode demonstrated a high specific capacity of 1220 mAh/g at a 0.1 C discharge rate. The sulfur cathode material also exhibits enhanced rate capability and cycling stability in comparison with sulfur composite which contains bulk sulfur particles and a relatively poor sulfur distribution. However, the improvement of cathode was largely limited by the component of amorphous carbon within the composite. This innovative synthesis method also faced some difficulties when applying to the mesoporous carbon-sulfur composite synthesis. Nevertheless, this synthesis approach still have the capability in other applications for sulfur containing composites synthesis, e.g. with other carbonaceous materials such as carbon nanotubes, graphene or polymers.

In general, the primary objectives of this research project are successfully achieved. The active mass utilization rate and rate capability of Li-S battery has been improved through modification of cathode component. My work of this project did not solve the problem of capacity degradation of sulfur cathode, but it could provide a new prospective to sulfur composite synthesis. Further works on improvement of cycle stability are essential for the development of Li-S battery.

References

1. Gabano, J.-P., ed. *Lithium Batteries*. 1983, Academic Press: New York.
2. Schalkwijk, W.A. and B. Scrosati, eds. *Advances in lithium-ion batteries*. 2002, Kluwer Academic/ Plenum Publishers: New York.
3. Jacobson, M.Z. and M.A. Delucchi, *Providing all global energy with wind, water, and solar power, Part I: Technologies, energy resources, quantities and areas of infrastructure, and materials.* Energy Policy, 2011. **39**(3): p. 1154-1169.
4. Delucchi, M.A. and M.Z. Jacobson, *Providing all global energy with wind, water, and solar power, Part II: Reliability, system and transmission costs, and policies.* Energy Policy, 2011. **39**(3): p. 1170-1190.
5. Scrosati, B. and J. Garche, *Lithium batteries: Status, prospects and future.* Journal of Power Sources, 2010. **195**(9): p. 2419-2430.
6. Goodenough, J.B. and Y. Kim, *Challenges for rechargeable batteries.* Journal of Power Sources, 2011. **196**(16): p. 6688-6694.
7. Manthiram, A., *Materials Challenges and Opportunities of Lithium Ion Batteries.* Journal of Physical Chemistry Letters, 2011. **2**(3): p. 176-184.
8. Eom, J.Y., et al., *Lithium insertion into purified and etched multi-walled carbon nanotubes synthesized on supported catalysts by thermal CVD.* Carbon, 2004. **42**(12-13): p. 2589-2596.
9. Mi, C.H., G.S. Cao, and X.B. Zhao, *A non-GIC mechanism of lithium storage in chemical etched MWNTs.* Journal of Electroanalytical Chemistry, 2004. **562**(2): p. 217-221.
10. Kaskhedikar, N.A. and J. Maier, *Lithium Storage ion Carbon Nanostructures.* Advanced Materials, 2009. **21**(25-26): p. 2664-2680.
11. Hassoun, J., et al., *A nanostructured Sn-C composite lithium battery electrode with unique stability and high electrochemical performance.* Advanced Materials, 2008. **20**(16): p. 3169-3175.
12. Todd, A.D.W., R.E. Mar, and J.R. Dahn, *Combinatorial study of tin-transition metal alloys as negative electrodes for lithium-ion batteries.* Journal of the Electrochemical Society, 2006. **153**(10): p. A1998-A2005.
13. Kim, H. and J. Cho, *Superior Lithium Electroactive Mesoporous Si@Carbon Core-Shell Nanowires for Lithium Battery Anode Material.* Nano Letters, 2008. **8**(11): p. 3688-3691.
14. Yoon, S. and A. Manthiram, *Nanoengineered Sn-TiC-C composite anode for lithium ion batteries.* Journal of Materials Chemistry, 2010. **20**(2): p. 236-239.
15. Huang, Z.L., et al., *Research Progress of Inorganic Sulfides Electrode Materials for Lithium-Ion Batteries.* Rare Metal Materials and Engineering, 2010. **39**(1): p. 182-188.
16. Obrovac, M.N., et al., *The electrochemical displacement reaction of lithium with metal oxides.* Journal of the Electrochemical Society, 2001. **148**(6): p. A576-A588.
17. Park, C.M., et al., *Li-alloy based anode materials for Li secondary batteries.* Chemical Society Reviews, 2010. **39**(8): p. 3115-3141.
18. Cabana, J., et al., *Beyond Intercalation-Based Li-Ion Batteries: The State of the Art and Challenges of Electrode Materials Reacting Through Conversion Reactions.* Advanced Materials, 2010. **22**(35): p. E170-E192.
19. Hu, Y.S., et al., *High lithium electroactivity of nanometer-sized rutile TiO2.* Advanced Materials, 2006. **18**(11): p. 1421-+.

20. Winter, M., et al., *Insertion electrode materials for rechargeable lithium batteries.* Advanced Materials, 1998. **10**(10): p. 725-763.
21. Yu, Y., et al., *Three-dimensional porous amorphous SnO(2) thin films as anodes for Li-ion batteries.* Electrochimica Acta, 2009. **54**(28): p. 7227-7230.
22. Lou, X.W., et al., *Preparation of SnO2/Carbon Composite Hollow Spheres and Their Lithium Storage Properties.* Chemistry of Materials, 2008. **20**(20): p. 6562-6566.
23. Poizot, P., et al., *Rationalization of the Low-Potential Reactivity of 3d-Metal-Based Inorganic Compounds toward Li.* Journal of the Electrochemical Society, 2002. **149**(9): p. A1212-A1217.
24. Poizot, P., et al., *Nano-sized transition-metaloxides as negative-electrode materials for lithium-ion batteries.* Nature, 2000. **407**(6803): p. 496-499.
25. Debart, A., et al., *Reactivity of transition metal (Co, Ni, Cu) sulphides versus lithium: The intriguing case of the copper sulphide.* Solid State Sciences, 2006. **8**(6): p. 640-651.
26. Yan, J.M., et al., *A study of novel anode material CoS2 for lithium ion battery.* Journal of Power Sources, 2005. **146**(1-2): p. 264-269.
27. Liu, B., et al., *Hydrothermal synthesis and magnetic properties of CoS(2) nano-octahedrons.* Materials Letters, 2011. **65**(17-18): p. 2804-2807.
28. Sadjadi, M.S., et al., *Formation of NiS and CoS semiconductor nanoparticles inside mordenite-type zeolite.* Materials Letters, 2007. **61**(14-15): p. 2923-2926.
29. Sun, X.C., et al., *Magnetic properties of a mixture of two nanosized Co-S powder's produced by hydrothermal reduction.* Ieee Transactions on Magnetics, 2003. **39**(5): p. 2678-2680.
30. Zhu, Y.F., D.H. Fan, and W.Z. Shen, *Chemical conversion synthesis and optical properties of metal sulfide hollow microspheres.* Langmuir, 2008. **24**(19): p. 11131-11136.
31. Bao, S.-J., et al., *Shape evolution and magnetic properties of cobalt sulfide.* Crystal Growth & Design, 2008. **8**(10): p. 3745-3749.
32. Luo, W., et al., *Spherical CoS(2)@ arbon core-shell nanoparticles: one-pot synthesis and Li storage property.* Nanotechnology, 2008. **19**(7).
33. Song, D.W., et al., *Liquid phase chemical synthesis of Co-S microspheres with novel structure and their electrochemical properties.* Journal of Power Sources, 2010. **195**(21): p. 7462-7465.
34. Wang, J., et al., *Synthesis and characterization of nanosize cobalt sulfide for rechargeable lithium batteries.* Journal of Power Sources, 2006. **159**(1): p. 287-290.
35. Wang, Q., et al., *Novel flower-like CoS hierarchitectures: one-pot synthesis and electrochemical properties.* Journal of Materials Chemistry, 2011. **21**(2): p. 327-329.
36. Momma, T., et al., *SnS2 anode for rechargeable lithium battery.* Journal of Power Sources, 2001. **97-8**: p. 198-200.
37. Seo, J.W., et al., *Two-Dimensional SnS(2) Nanoplates with Extraordinary High Discharge Capacity for Lithium Ion Batteries.* Advanced Materials, 2008. **20**(22): p. 4269-4273.
38. Liu, S.A., et al., *Synthesis of self-assembled 3D flowerlike SnS(2) nanostructures with enhanced lithium ion storage property.* Solid State Sciences, 2010. **12**(5): p. 712-718.
39. Chang, K., W.X. Chen, and H. Li, *Microwave-assisted synthesis of SnS(2)/SnO(2) composites by L-cysteine and their electrochemical performances when used as anode materials of Li-ion batteries.* Electrochimica Acta, 2011. **56**(7): p. 2856-2861.
40. Kim, H.S., et al., *Electrochemical behavior of carbon-coated SnS(2) for use as the anode in lithium-ion batteries.* Electrochimica Acta, 2009. **54**(13): p. 3606-3610.
41. Li, Y., et al., *Mechanochemical synthesis and electrochemical properties of nanosized SnS as*

an anode material for lithium ion batteries. Materials Science and Engineering B-Solid State Materials for Advanced Technology, 2006. **128**(1-3): p. 75-79.

42. Aso, K., A. Hayashi, and M. Tatsumisago, *Synthesis of Needle like and Platelike SnS Active Materials in High-Boiling Solvents and Their Application to All-Solid-State Lithium Secondary Batteries.* Crystal Growth & Design, 2011. **11**(9): p. 3900-3904.
43. Zhang, Y., et al., *Ultralarge single crystal SnS rectangular nanosheets.* Chemical Communications, 2011. **47**(18): p. 5226-5228.
44. Lai, C.-H., et al., *Direct growth of high-rate capability and high capacity copper sulfide nanowire array cathodes for lithium-ion batteries.* Journal of Materials Chemistry, 2010. **20**(32): p. 6638-6645.
45. Lai, C.-H., et al., *Oriented growth of large-scale nickel sulfide nanowire arrays via a general solution route for lithium-ion battery cathode applications.* Journal of Materials Chemistry, 2009. **19**(39): p. 7277-7283.
46. Chen, D., et al., *Aligned SnS2 nanotubes fabricated via a template-assisted solvent-relief process.* Applied Physics a-Materials Science & Processing, 2003. **77**(6): p. 747-749.
47. Ma, D., et al., *Controlled synthesis and possible formation mechanism of leaf-shaped SnS2 nanocrystals.* Materials Chemistry and Physics, 2008. **111**(2-3): p. 391-395.
48. Peng, J., et al., *Self-assembly of SnS(2) submicron-sized flakes to form microspheres under template-free hydrothermal conditions.* Journal of Alloys and Compounds, 2010. **490**(1-2): p. L20-L23.
49. Hu, Q.R., et al., *Synthesis of cobalt sulfide nanostructures by a facile solvothermal growth process.* Journal of Alloys and Compounds, 2010. **491**(1-2): p. 707-711.
50. Chakrabarti, A., et al., *Tin(IV) sulfide: Novel nanocrystalline morphologies.* Inorganica Chimica Acta, 2011. **374**(1): p. 627-631.
51. Girishkumar, G., et al., *Lithium - Air Battery: Promise and Challenges.* Journal of Physical Chemistry Letters, 2010. **1**(14): p. 2193-2203.
52. Ji, X. and L.F. Nazar, *Advances in Li-S batteries.* Journal of Materials Chemistry, 2010. **20**(44): p. 9821-9826.
53. Cheon, S.E., et al., *Rechargeable lithium sulfur battery - I. Structural change of sulfur cathode during discharge and charge.* Journal of the Electrochemical Society, 2003. **150**(6): p. A796-A799.
54. Cheon, S.E., et al., *Rechargeable lithium sulfur battery - II. Rate capability and cycle characteristics.* Journal of the Electrochemical Society, 2003. **150**(6): p. A800-A805.
55. Mikhaylik, Y.V. and J.R. Akridge, *Polysulfide shuttle study in the Li/S battery system.* Journal of the Electrochemical Society, 2004. **151**(11): p. A1969-A1976.
56. Ryu, H.S., et al., *Self-discharge characteristics of lithium/sulfur batteries using TEGDME liquid electrolyte.* Electrochimica Acta, 2006. **52**(4): p. 1563-1566.
57. Ryu, H.S., et al., *Self-discharge of lithium-sulfur cells using stainless-steel current-collectors.* Journal of Power Sources, 2005. **140**(2): p. 365-369.
58. Chang, D.R., et al., *Binary electrolyte based on tetra(ethylene glycol) dimethyl ether and 1,3-dioxolane for lithium-sulfur battery.* Journal of Power Sources, 2002. **112**(2): p. 452-460.
59. Smart, M.C., B.V. Ratnakumar, and S. Surampudi, *Use of organic esters as cosolvents in electrolytes for lithium-ion batteries with improved low temperature performance.* Journal of the Electrochemical Society, 2002. **149**(4): p. A361-A370.

60. Kolosnitsyn, V.S., et al., *Cycling lithium-sulfur batteries.* Russian Journal of Electrochemistry, 2002. **38**(3): p. 329-331.
61. Wagner, M.W., C. Liebenow, and J.O. Besenhard, *Effect of polysulfide-containing electrolyte on the film formation of the negative electrode.* Journal of Power Sources, 1997. **68**(2): p. 328-332.
62. Kim, S., Y.J. Jung, and H.S. Lim, *The effect of solvent component on the discharge performance of Lithium-sulfur cell containing various organic electrolytes.* Electrochimica Acta, 2004. **50**(2-3): p. 889-892.
63. Zhu, X.J., et al., *Electrochemical characterization and performance improvement of lithium/sulfur polymer batteries.* Journal of Power Sources, 2005. **139**(1-2): p. 269-273.
64. Marmorstein, D., et al., *Electrochemical performance of lithium/sulfur cells with three different polymer electrolytes.* Journal of Power Sources, 2000. **89**(2): p. 219-226.
65. Shin, J.H., et al., *Electrochemical properties and interfacial stability of (PEO)(10)LiCF3SO3-TinO2n-1 composite polymer electrolytes for lithium/sulfur battery.* Materials Science and Engineering B-Solid State Materials for Advanced Technology, 2002. **95**(2): p. 148-156.
66. Aurbach, D., et al., *THE ELECTROCHEMICAL-BEHAVIOR OF 1,3-DIOXOLANE-LICLO4 SOLUTIONS .1. UNCONTAMINATED SOLUTIONS.* Electrochimica Acta, 1990. **35**(3): p. 625-638.
67. Kolosnitsyn, V.S., E.V. Karaseva, and A.L. Ivanov, *Electrochemistry of a lithium electrode in lithium polysulfide solutions.* Russian Journal of Electrochemistry, 2008. **44**(5): p. 564-569.
68. Yuan, L.X., et al., *Improved dischargeability and reversibility of sulfur cathode in a novel ionic liquid electrolyte.* Electrochemistry Communications, 2006. **8**(4): p. 610-614.
69. Choi, Y.-J., et al., *Improvement of cycle property of sulfur electrode for lithium/sulfur battery.* Journal of Alloys and Compounds, 2008. **449**(1-2): p. 313-316.
70. Ryu, H.S., et al., *Investigation of discharge reaction mechanism of lithium vertical bar liquid electrolyte vertical bar sulfur battery.* Journal of Power Sources, 2009. **189**(2): p. 1179-1183.
71. Yamin, H., et al., *LITHIUM SULFUR BATTERY - OXIDATION REDUCTION-MECHANISMS OF POLYSULFIDES IN THF SOLUTIONS.* Journal of the Electrochemical Society, 1988. **135**(5): p. 1045-1048.
72. Shin, J.H. and E.J. Cairns, *N-Methyl-(n-butyl)pyrrolidinium bis(trifluoromethanesulfonyl)imide-LiTFSI-poly(ethylene glycol) dimethyl ether mixture as a Li/S cell electrolyte.* Journal of Power Sources, 2008. **177**(2): p. 537-545.
73. Trofimov, B.A., et al., *Protected bis(hydroxyorganyl) polysulfides as modifiers of Li/S battery electrolyte.* Electrochimica Acta, 2011. **56**(5): p. 2458-2463.
74. Choi, J.-W., et al., *Rechargeable lithium/sulfur battery with liquid electrolytes containing toluene as additive.* Journal of Power Sources, 2008. **183**(1): p. 441-445.
75. Choi, J.-W., et al., *Rechargeable lithium/sulfur battery with suitable mixed liquid electrolytes.* Electrochimica Acta, 2007. **52**(5): p. 2075-2082.
76. Wang, J.L., et al., *Sulfur-carbon nano-composite as cathode for rechargeable lithium battery based on gel electrolyte.* Electrochemistry Communications, 2002. **4**(6): p. 499-502.
77. Wang, J., et al., *Sulfur-mesoporous carbon composites in conjunction with a novel ionic liquid electrolyte for lithium rechargeable batteries.* Carbon, 2008. **46**(2): p. 229-235.
78. Yuan, L., et al., *Improvement of cycle property of sulfur-coated multi-walled carbon nanotubes composite cathode for lithium/sulfur batteries.* Journal of Power Sources, 2009.

189(2): p. 1141-1146.

79. Wu, F., et al., *Electrochemical performance of sulfur composite cathode materials for rechargeable lithium batteries.* Chinese Chemical Letters, 2009. **20**(10): p. 1255-1258.
80. Aurbach, D., et al., *On the Surface Chemical Aspects of Very High Energy Density, Rechargeable Li-Sulfur Batteries.* Journal of the Electrochemical Society, 2009. **156**(8): p. A694-A702.
81. Liang, X., et al., *Highly dispersed sulfur in ordered mesoporous carbon sphere as a composite cathode for rechargeable polymer Li/S battery.* Journal of Power Sources, 2011. **196**(7): p. 3655-3658.
82. Shin, J.H., et al., *Preparation and characterization of plasticized polymer electrolytes based on the PVdF-HFP copolymer for lithium/sulfur battery.* Journal of Materials Science-Materials in Electronics, 2002. **13**(12): p. 727-733.
83. Hassoun, J. and B. Scrosati, *Moving to a Solid-State Configuration: A Valid Approach to Making Lithium-Sulfur Batteries Viable for Practical Applications.* Advanced Materials, 2010. **22**(45): p. 5198-+.
84. Wei, W., et al., *CNT enhanced sulfur composite cathode material for high rate lithium battery.* Electrochemistry Communications, 2011. **13**(5): p. 399-402.
85. Chen, J.-j., et al., *The preparation of nano-sulfur/MWCNTs and its electrochemical performance.* Electrochimica Acta, 2010. **55**(27): p. 8062-8066.
86. Han, S.C., et al., *Effect of multiwalled carbon nanotubes on electrochemical properties of lithium sulfur rechargeable batteries.* Journal of the Electrochemical Society, 2003. **150**(7): p. A889-A893.
87. Zheng, W., et al., *Novel nanosized adsorbing sulfur composite cathode materials for the advanced secondary lithium batteries.* Electrochimica Acta, 2006. **51**(7): p. 1330-1335.
88. Ryoo, R., S.H. Joo, and S. Jun, *Synthesis of highly ordered carbon molecular sieves via template-mediated structural transformation.* Journal of Physical Chemistry B, 1999. **103**(37): p. 7743-7746.
89. Lee, J., J. Kim, and T. Hyeon, *Recent progress in the synthesis of porous carbon materials.* Advanced Materials, 2006. **18**(16): p. 2073-2094.
90. Grigoriants, I., et al., *The use of tin-decorated mesoporous carbon as an anode material for rechargeable lithium batteries.* Chemical Communications, 2005(7): p. 921-923.
91. Ji, X., et al., *Carbon/MoO2 composite based on porous semi-graphitized nanorod assemblies from in situ reaction of tri-block polymers.* Chemistry of Materials, 2007. **19**(3): p. 374-383.
92. Lai, C., et al., *Synthesis and Electrochemical Performance of Sulfur/Highly Porous Carbon Composites.* Journal of Physical Chemistry C, 2009. **113**(11): p. 4712-4716.
93. Jayaprakash, N., et al., *Porous Hollow Carbon@Sulfur Composites for High-Power Lithium-Sulfur Batteries.* Angewandte Chemie-International Edition, 2011. **50**(26): p. 5904-5908.
94. He, X., et al., *Expansion and shrinkage of the sulfur composite electrode in rechargeable lithium batteries.* Journal of Power Sources, 2009. **190**(1): p. 154-156.
95. Liang, C., N.J. Dudney, and J.Y. Howe, *Hierarchically Structured Sulfur/Carbon Nanocomposite Material for High-Energy Lithium Battery.* Chemistry of Materials, 2009. **21**(19): p. 4724-4730.
96. Wang, C., et al., *Preparation and performance of a core-shell carbon/sulfur material for lithium/sulfur battery.* Electrochimica Acta, 2010. **55**(23): p. 7010-7015.

97. Yu, X.U., et al., *Stable-cycle and high-capacity conductive sulfur-containing cathode materials for rechargeable lithium batteries.* Journal of Power Sources, 2005. **146**(1-2): p. 335-339.
98. Kim, H., et al., *SnO(2)/Graphene Composite with High Lithium Storage Capability for Lithium Rechargeable Batteries.* Nano Research, 2010. **3**(11): p. 813-821.
99. Liang, Y.Y., et al., *TiO(2) Nanocrystals Grown on Graphene as Advanced Photocatalytic Hybrid Materials.* Nano Research, 2010. **3**(10): p. 701-705.
100. Wang, D.H., et al., *Self-Assembled TiO(2)-Graphene Hybrid Nanostructures for Enhanced Li-Ion Insertion.* Acs Nano, 2009. **3**(4): p. 907-914.
101. Wang, H.L., et al., *Mn(3)O(4)-Graphene Hybrid as a High-Capacity Anode Material for Lithium Ion Batteries.* Journal of the American Chemical Society, 2010. **132**(40): p. 13978-13980.
102. Wang, H.L., et al., *Advanced asymmetrical supercapacitors based on graphene hybrid materials.* Nano Research, 2011. **4**(8): p. 729-736.
103. Wang, H.L., et al., *Ni(OH)(2) Nanoplates Grown on Graphene as Advanced Electrochemical Pseudocapacitor Materials.* Journal of the American Chemical Society, 2010. **132**(21): p. 7472-7477.
104. Wang, X.R., S.M. Tabakman, and H.J. Dai, *Atomic layer deposition of metal oxides on pristine and functionalized graphene.* Journal of the American Chemical Society, 2008. **130**(26): p. 8152-+.
105. Yang, S.B., et al., *Fabrication of Cobalt and Cobalt Oxide/Graphene Composites: Towards High-Performance Anode Materials for Lithium Ion Batteries.* Chemsuschem, 2010. **3**(2): p. 236-239.
106. Xiao, J., et al., *Hierarchically porous graphene as a lithium-air battery electrode.* Nano Letters, 2011. **11**(11): p. 5071-8.
107. Yoo, E. and H. Zhou, *Li-Air Rechargeable Battery Based on Metal-free Graphene Nanosheet Catalysts.* Acs Nano, 2011. **5**(4): p. 3020-3026.
108. Rui, X., et al., *Reduced graphene oxide supported highly porous V(2)O(5) spheres as a high-power cathode material for lithium ion batteries.* Nanoscale, 2011. **3**(11): p. 4752-4758.
109. Li, Y., et al., *Superior energy capacity of graphene nanosheets for a nonaqueous lithium-oxygen battery.* Chemical Communications, 2011. **47**(33): p. 9438-9440.
110. Wang, H., et al., *Graphene-Wrapped Sulfur Particles as a Rechargeable Lithium-Sulfur Battery Cathode Material with High Capacity and Cycling Stability.* Nano Letters, 2011. **11**(7): p. 2644-2647.
111. Cao, Y., et al., *Sandwich-type functionalized graphene sheet-sulfur nanocomposite for rechargeable lithium batteries.* Physical Chemistry Chemical Physics, 2011. **13**(17): p. 7660-7665.
112. Wang, J.-Z., et al., *Sulfur-graphene composite for rechargeable lithium batteries.* Journal of Power Sources, 2011. **196**(16): p. 7030-7034.
113. Qiu, L., et al., *Preparation and enhanced electrochemical properties of nano-sulfur/poly(pyrrole-co-aniline) cathode material for lithium/sulfur batteries.* Electrochimica Acta, 2010. **55**(15): p. 4632-4636.
114. Ji, X., K.T. Lee, and L.F. Nazar, *A highly ordered nanostructured carbon-sulphur cathode for lithium-sulphur batteries.* Nature Materials, 2009. **8**(6): p. 500-506.
115. Cains, P.W., P.D. Martin, and C.J. Price, *The use of ultrasound in industrial chemical synthesis and crystallization. 1. Applications to synthetic chemistry.* Organic Process Research &

Development, 1998. **2**(1): p. 34-48.
116. Gedanken, A., *Using sonochemistry for the fabrication of nanomaterials.* Ultrasonics Sonochemistry, 2004. **11**(2): p. 47-55.
117. Hummers, W.S. and R.E. Offeman, *PREPARATION OF GRAPHITIC OXIDE.* Journal of the American Chemical Society, 1958. **80**(6): p. 1339-1339.
118. Wang, G., et al., *Graphene nanosheets for enhanced lithium storage in lithium ion batteries.* Carbon, 2009. **47**(8): p. 2049-2053.
119. Choi, Y.S., et al., *Effect of cathode component on the energy density of lithium-sulfur battery.* Electrochimica Acta, 2004. **50**(2-3): p. 833-835.
120. Jun, S., et al., *Synthesis of new, nanoporous carbon with hexagonally ordered mesostructure.* Journal of the American Chemical Society, 2000. **122**(43): p. 10712-10713.

Definitions

A **battery** is one or more electrically connected electrochemical cells having terminals/contacts to supply electrical energy.

A **supercapacitor** is a device that stores electrical energy in the electrical double layer that forms at the interface between an electrolytic solution and an electronic conductor.

The **anode** is the negative electrode of a cell associated with oxidative chemical reactions that release electrons into the external circuit.

The **cathode** is the positive electrode of a cell associated with reductive chemical reactions that gain electrons from the external circuit.

A **separator** is a physical barrier between the positive and negative electrodes incorporated into most cell designs to prevent electrical shorting. The separator can be a gel-electrolyte or a porous material (e.g. polypropylene) filled with electrolyte. Separators must be permeable to the ions and inert to electrolyte and electrode species.

Discharge is an operation in which a battery delivers electrical energy to an external load.

Charge is an operation in which a battery is restored to its original charged condition through the reversal of external current flow.

Coulombic efficiency is the ratio between the energy removed from a battery during discharge compared with the energy used during charging to restore the original capacity.

Working electrode is an electrode at which the reaction of interest occurs.

Counter electrode is the current-carrying partner of the working electrode.